Principles of Surface-based Microwave and Millimeter wave Radiometric Remote Sensing of the Troposphere

Ed R. Westwater[1], Susanne Crewell[2], Christian Mätzler[3], and Domenico Cimini[1,4]

Abstract - Surface-based radiometric measurements of tropospheric parameters have long provided useful measurements of temperature, water vapor, and cloud liquid. In this paper, a general overview of physical fundamentals, measurement techniques, and retrieval methodology is given. Then several contemporary instruments are discussed and representative results are presented. Recent and promising developments include multi-frequency radiometers, scanning observations of clouds, and combined active-passive remote sensing. The primary applications of these new technologies are weather forecasting and climate, communications, geodesy and long-baseline interferometry, satellite data validation, air-sea interaction, and fundamental molecular physics. The work presented here updates and extends the reviews published in [11] and [37].

I. INTRODUCTION

Surface-based radiometric measurements of atmospheric thermal emission are useful in a variety of meteorological applications, including meteorological observations and forecasting, communications, geodesy and long-baseline interferometry, satellite validation, climate, air-sea interaction, and fundamental molecular physics. One reason for the utility of these measurements is that with careful design, radiometers can be operated in a long-term unattended mode in nearly all weather conditions [1, 2, 3]. An important feature is the nearly continuous observational capability on time scales of seconds to minutes. The measurements can enable the continued development of absorption and radiative transfer models in both clear [4, 5] and cloudy [6] atmospheres. This development has been greatly

---

1 Cooperative Institute for Research in Environmental Sciences, University of Colorado/ NOAA ESRL Physical Science Division 325 Broadway MS R/PSD4,Boulder, CO 80305 USA
2 Meteorologisches Institut, Universitaet Muenchen, Theresienstr. 37, 80333 Muenchen, Germany
3 Institute of Applied Physics, University of Bern, Sidlerstr. 5, CH-3012 Bern, Switzerland
4 Institute of Methodologies for Environmental Analysis, National Research Council, Tito Scalo (PZ), 85050, Italy.

aided by long-term, carefully calibrated radiometer measurements, supplemented by frequent radiosonde releases using active sensors for cloud identification [7, 8]. Last, but not least, is the development of retrieval and data assimilation algorithms [9, 10] with which radiometer data can be combined with external data sources, such as forecasts or soundings from active sensors. In this paper on surface-based radiometers and their meteorological products, we confine our attention to radiometric measurements of water vapor, temperature, and clouds in the troposphere. More extensive reviews are given in [11, 37] and some of the material in this overview has been extracted from these documents.

II. General Physical Principles

The basic ideas of radiative transfer and thermal emission are given in [12] and their application to microwave radiometric remote sensing is outlined in [13]. From the concept of an ideal black body and Kirchoff's law, it is known that the emission from a black body depends only on its temperature and that the higher the temperature of the body, the more is its emission. The idea is made quantitative by calculating the spectral distribution of a blackbody emission from Planck's law, which expresses the radiance $B_v(T)$ emitted from a blackbody at temperature T and frequency v as

$$B_v(T) = \frac{2hv^3}{c^2} \frac{1}{(\exp(hv/kT)-1)}$$

(1)

where h = Planck's constant, and k = Boltzman's constant. The radiance expresses the emitted power per unit projected area per unit solid angle per unit frequency interval. The second consideration is to relate the emission from a real body, sometimes called a "grey" body, to that of a blackbody at the same temperature. If the fraction of incident energy from a certain direction absorbed by the grey body is $A(v)$, then the amount emitted is $A(v) B_v(T)$. For a perfectly reflecting or transmitting body, $A(v)$ is zero, and incident energy may be redirected or pass through the body without being absorbed. In the situation considered here, namely upward-looking radiometers viewing a non-scattering medium, the equation that relates our primary observable, brightness temperature, T_b, to the atmospheric state is the radiative transfer equation (RTE) [13]

$$B_v(T_b) = B_v(T_c)\exp(-\tau_v) + \int_0^\infty B_v(T(s))\,\alpha_v(s)\exp(-\int_0^s \alpha_v(s')ds')\,ds,$$

(2a)

where s = path length in km, $T(s)$ = Temperature (K) at the point s, T_c = Cosmic background brightness temperature of 2.75 K, τ_v = opacity = total optical depth along the path

$$\tau_v = \int_0^\infty \alpha_v(s)\,ds,$$

(2b)

where $\alpha_\nu(s)$ = absorption coefficient (nepers/km) at the point s. The use of the blackbody source function in (2a) is justified by the assumption of local thermodynamic equilibrium in which the population of emitting energy states is determined by molecular collisions and is independent of the incident radiation field [12].

Equation (2) and its Rayleigh-Jeans approximation are discussed in [13], and its more general form including scattering is discussed in [14]. Scattering, although neglected here, may arise from liquid, ice, or melting liquid depending on the size distribution of the particles. For our purposes, we note the dependence on the temperature profile $T(s)$ and the implicit dependence on pressure, water vapor, and cloud liquid through $\alpha_\nu(s)$. For a plane parallel atmosphere, s and the height h are related by $s \cdot sin(\theta) = h$, where θ is the elevation angle. Information on meteorological variables is obtained from measurements of T_b as a function of ν and/or θ. Equation (2) is used: (a) in forward model studies in which the relevant meteorological variables are measured by radiosonde in situ soundings, (b) in inverse problems and parameter retrieval applications, in which meteorological information is inferred from measurements of T_b or τ, and (c) in system modeling studies for determining the effects of instrument noise on retrievals and optimum measurement ordinates, such as ν and θ. Calculations of T_b for a warm (surface temperature T_s =293 K) atmosphere are shown in Figure 1. The region around 22.235 GHz is used for sensing of water vapor, while the transmission windows near 30-50, 70-100, and 130-150 GHz are used primarily for remote sensing of clouds. The strong absorption regions near 60 and 118 GHz are used for temperature sensing. Finally, the strong absorption region near 183 GHz is used to study very low amounts of water vapor such as are found during Arctic winter conditions.

III. MICROWAVE ABSORPTION AND EMISSION

The principal sources of atmospheric microwave emission and absorption are water vapor, oxygen, and cloud liquid. In the frequency region from 20 to 200 GHz, water-vapor absorption arises from the weak electric dipole rotational transition at 22.235 GHz and the much stronger transition at 183.31 GHz. In addition, the so-called continuum absorption of water vapor arises from the far wing contributions from higher-frequency resonances that extend into the infrared region. Again, in the frequency band from 20 to 200 GHz, oxygen absorbs due to a series of magnetic dipole transitions centered around 60 GHz and the isolated line at 118.75 GHz. Because of pressure broadening, i.e., the effect of molecular collisions on radiative transitions, both water vapor and oxygen absorption extend outside of the immediate frequency region of their resonant lines. There are also resonances by ozone that are important for stratospheric sounding [15]. In addition to gaseous absorption, scattering, absorption, and emission also originate from hydrometeors in the atmosphere. Our focus in this article is on non-precipitating clouds for which emission and absorption are of primary importance.

III.1. Gaseous Absorption Models

Detailed calculations of absorption by water vapor and oxygen were first published by J. H. Van Vleck [16, 17]. The quantum mechanical basis of these calculations, including the Van Vleck-Weisskopf line shape [18], together with laboratory measurements, has led to increasingly accurate calculations of gaseous absorption. Both these historical- and recent- developments are discussed in [19]. Currently, there are several absorption models that are widely used in the propagation and remote-sensing communities. Starting with laboratory measurements that were made in the late 1960s and continuing for several years, H. Liebe developed and distributed the computer code of his Microwave Propagation Model (MPM). One version of the model [20] is still used extensively, and many subsequent models are compared with this one. Liebe later made changes to both water-vapor and oxygen models, especially to parameters describing the 22.235 GHz H2O line and the so-called water vapor continuum [21]. More recently, Rosenkranz [5a, 5b] developed an improved absorption model that also is extensively used in the microwave propagation community. However, there are many issues in the determination of parameters that enter into water-vapor-absorption modeling, and a clear discussion of several of these issues is given in [19]. Relevant to the discussion is the choice of parameters to calculate the pressure-broadened line width, which, in the case of water vapor, arises from the collisions of H_2O with other H_2O molecules (self broadening), or from collisions of H_2O molecules with those of dry air (foreign broadening). In fact, Rosenkranz [5a, 5b] based his model on using Liebe and Layton's [20] values for the foreign-broadened component, and those from Liebe et al. [21] for the self-broadened component. Another model that is used extensively in the US climate research community is the Line by Line Radiative Transfer Model (LBLRTM) by S. Clough and his colleagues [7, 83]. An extension of the model, called MONORTM, is most appropriate for millimeter wave and microwave RTE studies [83]. One feature of the Clough models is that they have been compared extensively with simultaneous radiation and radiosonde observations near 20 and 30 GHz. Recently, two important refinements of absorption models have occurred. This first is the Rosenkranz [22, 84, 85] refinement of his 1998 codes. The second is by Liljegren et al. [23], which incorporates the line width parameters of the 22.235 GHz model from the HITRAN data base [86] with a different continuum formalization. Both of these new models show initial promise in calculating emission from radiosonde data [24].

III.2. Cloud Absorption Models

For spherical particles, the classical method to calculate scattering and absorption coefficients is through the Lorenz-Mie Equations [25, 26, 27]; for sufficiently small particles, the Rayleigh approximation can be used. For a given wavelength and single particle, the particle contribution is calculated; the total coefficients are then obtained by integration over the size distribution of particles. An important physical property for the calculations is the complex dielectric constant of the particle. This dielectric constant of liquid water is described by the dielectric relaxation spectra of Debye [28].
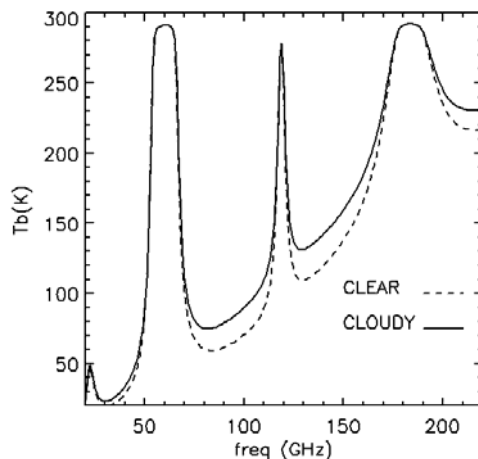
Figure 1 - *Calculated brightness temperatures (K) from 20 to 220 GHz for clear and cloudy conditions. The clear calculations are based on a standard atmosphere with the surface values (S) of P_S =1013 mb, T_S =293 K, ρ_S = 10 gm^{-3}, and PWV = 2.34 cm. The cloudy atmosphere contains 1 mm of integrated cloud liquid with a cloud layer of liquid density of 0.1 gm^{-3} between 1 and 2 km. The absorption models used are given in Figure 2.*
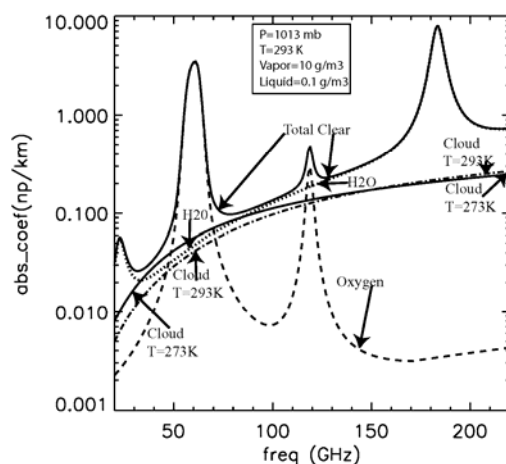

Figure 2 - *Microwave absorption spectra from 20 to 220 GHz. The absorption models used were Liebe 89 [4] for clear absorption, and Liebe et al. 1991 [6] for cloud liquid. P = pressure, T = temperature, ρ_V = absolute humidity, and ρ_L = cloud liquid density.*

The strong temperature dependence of the relaxation frequency is linked to the temperature-dependent viscosity of liquid water; therefore the cloud-absorption coefficient also shows significant temperature sensitivity. Above 0 °C, the dielectric constant can be well measured in the laboratory, and a variety of measurements have been made from 5 to 500 GHz [6]. However for super-cooled water, below 0 °C, the situation is less certain, and, for example, models of [6, 29, 30] differ by 20 to 30% in this region [31]. This is relevant for cloud remote sensing, because measurements

of super-cooled liquid are important for detection of aircraft icing [32]. When calculating absorption for nonprecipitating clouds, we assume Rayleigh absorption, for which the liquid absorption depends only on the total liquid amount and does not depend on the drop size distribution, and scattering is negligible. The Rayleigh approximation is valid when the scattering parameter $\beta=|n(2\pi r/\lambda)| \ll 1$ [26]. Here, r is the particle radius, λ is the free space wavelength, and n is the complex refractive index. For rain and other situations for which the β is greater than roughly 0.1, the full Mie equations, combined with a modeled (or measured) size distribution, must be used. Due to the nonspherical shape of ice hydrometeors, the situation is more complicated when scattering plays a role. Although this situation is beyond the scope of this article, the particle size of cirrus clouds can be of the order of 100 to 200 microns, and scattering may be important near transmission windows at millimeter wavelengths. On the other hand, the dielectric properties of ice [33, 34] are very different from those of liquid water. The dielectric losses of ice have a minimum near 1 GHz, and ice is an almost perfectly loss-free medium over a large frequency range. Therefore microwave emission of pure ice particles can be neglected in most cloud situations. Special situations occur when ice particles start to melt. A very thin skin of liquid water can be sufficient to cause significant absorption and thus emission. Usually, these conditions apply to precipitating clouds or in the so-called radar "bright band."

III.3. Calculations of Absorption Spectra

For standard conditions at sea level, we calculated the water vapor (H_2O), oxygen (O_2), and total clear ($H_2O + O_2$) contributions to the absorption coefficient. In addition, we calculated the liquid absorption coefficient for $\rho_L = 0.1$ gm^{-3} at $T=$ 293 and 273 K. From the results shown in Figure 2, we note the strong oxygen absorption regions near 60 and 118 GHz and the large absorption near 183 GHz due to water vapor. For a given location and altitude, the oxygen absorption is relatively constant, with variations of 10 to 20%, while both the 22.235 and the 183.31 GHz absorptions can vary by a factor of 10 to 20. Note also the strong temperature dependence of cloud absorption, and the reversal of this dependence at around 150 GHz.

III.4. Radiometric Response to Atmospheric Profiles: Weighting Functions

Equations (2) describe the theoretical radiometric response to atmospheric temperature T(s) and absorption coefficient $\alpha_v(s)$ as a function of the path coordinate s. The absorption coefficient, in turn, is a function of T(s), pressure P(s), water vapor density $\rho_V(s)$, and cloud liquid density $\rho_L(s)$. As discussed in Section III.2, we are assuming conditions for which the Rayleigh approximation is valid. In general, the response $B_v(T_b)$ to profiles is a nonlinear functional of T, P, ρ_V, and ρ_L, i.e. $B_v = B_v\{T, P, \rho_V, \rho_L\}$.
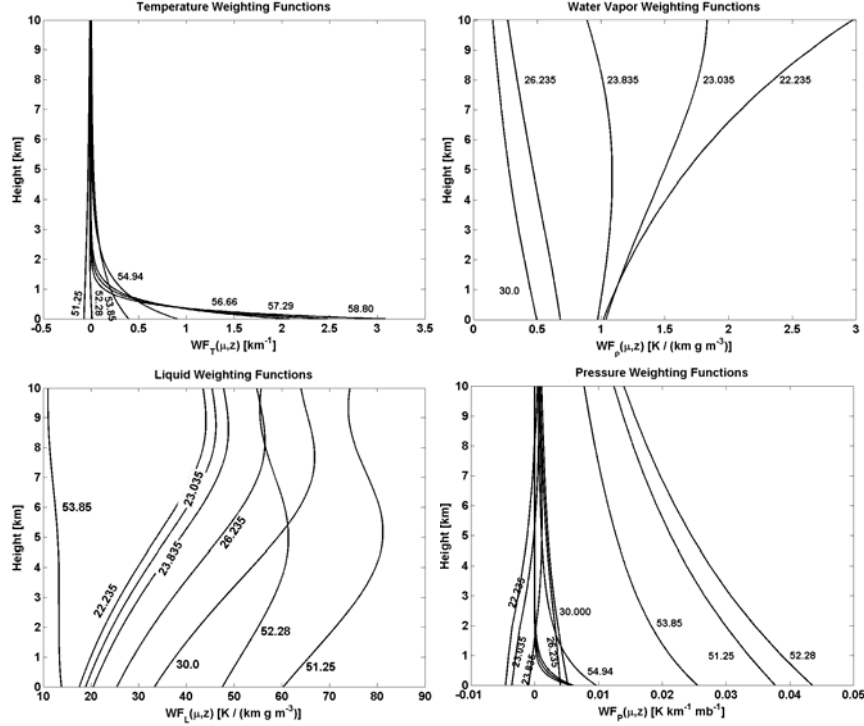
Figure 3 - Weighting functions for the Radiometrics Corporation MWRP. 3A. Temperature weighting functions and center frequencies for V-band channels. High sensitivity to boundary layer temperatures is shown. 3B. Vapor density weighting functions and center frequencies for K-band channels. In conjunction with typical vapor density scale height of approximately 2 km, the vapor density weighting functions provide substantial constraints in the boundary layer. 3C. Liquid density weighting functions for K1-5 and V1-3. The relatively large weighting functions in (a) indicate the K and lower V-band brightness temperature measurements provide significant constraints on the liquid density retrieval. 3D. Pressure weighting functions for all 12-channel. Note that for V1-3, pressure fluctuations are not negligible.

However, it is quite revealing to consider the response in B_ν to small changes in an initial state or background profiles. Thus, if we denote these background profiles as $\{T_0, P_0, \rho_{V0}, \rho_{L0}\}$, then we can write

$$\delta B_\nu = \int_0^\infty (W_T(s)\,\delta T(s) + W_P(s)\delta P(s) + W_{\rho_V}(s)\delta\rho_V(s) + W_{\rho_L}(s)\delta\rho_L(s))ds \quad (3)$$

where the weighting functions W can be explicitly calculated from the dependence of $\alpha_\nu(s)$ on the background profiles. For simplicity in notation, we have suppressed the frequency dependence of W. Further discussion on the calculation of weighting functions and their significance can be found in [14, 40].

In sections V, VI, and VII, we present instruments and techniques for remote sensing of atmospheric variables. Here, we will show representative weighting functions for many of these techniques.

III.4.1. Temperature Weighting Functions near 60 GHz

In section VI.5, we discuss the Microwave Radiometer Profiler manufactured by Radiometrics Corporation of the USA. The Temperature Weighting Functions for this instrument are similar to other multi-frequency radiometers that use the 60 GHz O_2 emission band and are shown in Figure 3a. Note the significantly different response of the first four channels to temperature in the first 2 km, and the lack of significantly different response above this altitude.

III.4.2. Water Vapor Weighting Functions near 22.235 GHz

The MWRP also contains 5 channels for water vapor and cloud liquid density sensing; the corresponding Water Vapor Weighting Functions are shown in Figure 3b. We note that the 22.235 and 22.035 GHz weighting functions increase with height, while the 23.835 GHz function is almost constant with height. The constant response with height implies that the channel is the most appropriate to derive Precipitable Water Vapor (PWV)–the total amount of water vapor in a column of unit cross section:

$$PWV = \int_0^\infty \rho_V \, dh \qquad (4)$$

In Equation (4) we have chosen the atmospheric path variable s as the height above the surface h. Measurements of T_b from the five channels can be used to infer coarse vertical features of the water vapor profile (see Section VII).

III.4.3. Pressure Weighting Functions below 60 GHz

Because of pressure broadening, the variations in pressure from an initial state can also give rise to changes to T_b (see Figure 3c). Although changes in P_0 of, say 1 mb, give a maximum of 0.045 K, a not uncommon 10 mb change gives a 0.45 K change in T_b which is not generally negligible. This suggests that when considering a background state that represents an entire month of observations, supplementing T_b with surface pressure measurements would be quite useful.

III.4.4. Cloud Liquid Weighting Functions below 60 GHz

As shown in Figure 3d, both the lower five channels of the MWRP and two of the upper seven channels contain significant response to cloud liquid water density. These functions, derived for cloud-droplet sizes in the Rayleigh region, indicate that brightness temperature measurements can be used to infer coarse vertical features of the liquid water profile (see Section VII). However, such measurements supplemented with additional measurements of cloud base and top from active sensors [77] can be used for profiling of ρ_L.
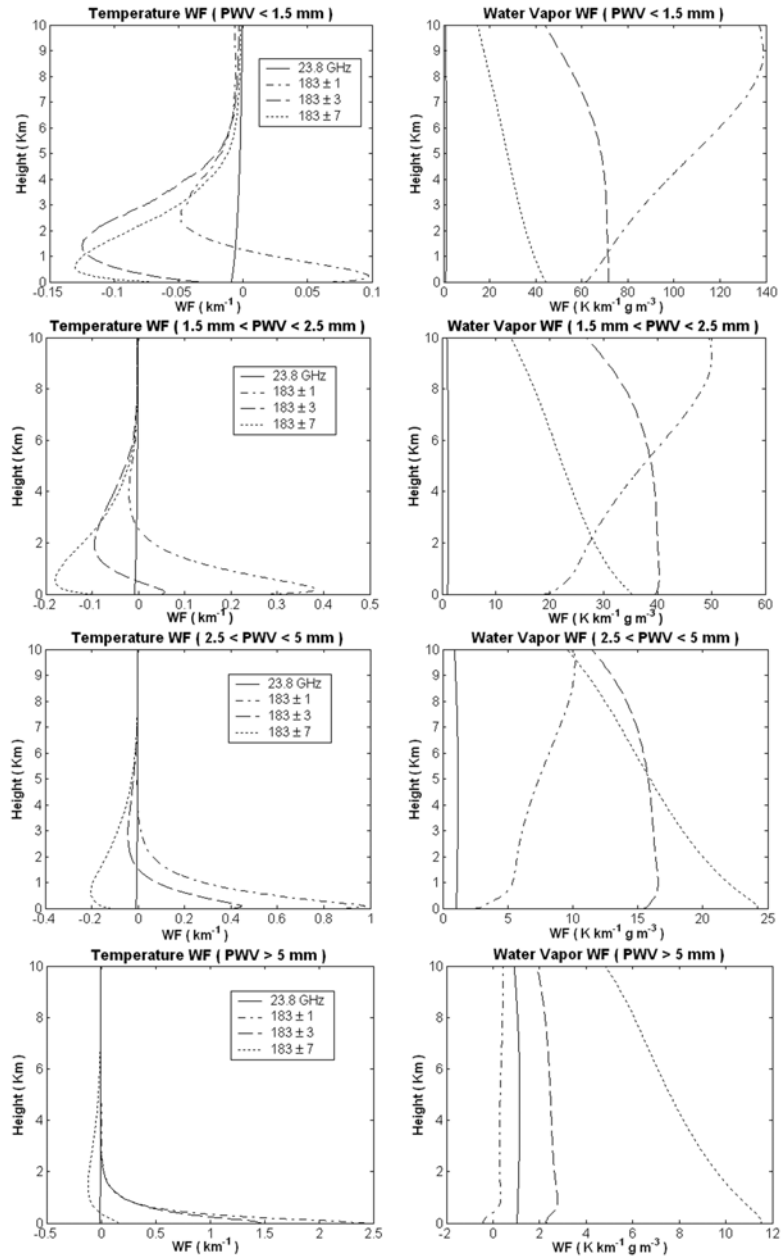
Figure 4 - *Average vapor density and temperature weighting functions for four ranges of PWV. The absorption model used is Rosenkranz [5]. After [36].*

III.4.5. Temperature and Water Vapor Weighting Functions at Millimeter Wavelengths

For cold temperatures (-20 to -40ºC) and dry conditions (PWV $< \sim 0.5$ g/cm^2), the sensitivity of brightness temperature measurements near 22.235 GHz to water vapor is not high. A way to overcome this lack of sensitivity is to measure brightness temperature near 183.31 GHz. As shown in Figure 2, the absorption near 183.31 GHz is significantly larger (from 10 to 100 times greater, depending on the exact frequency). However, because of the strength of the 183.31 GHz line, the response to water vapor and temperature is nonlinear and can change significantly depending on the amount of water vapor present in the atmosphere. Thus, instead of weighting functions that are linear over a broad range of atmospheric conditions, the response functions depend markedly on the amount of water vapor present. This nonlinear response is illustrated in Figure 4, in which both W_T and W_{ρ_V} are shown for several ranges of PWV.

IV. RETRIEVAL TECHNIQUES

Techniques to derive meteorological information from radiation measurements are generally based on Equations (2) or its perturbation form Equation (3). Because only a finite number of imperfect radiation measurements are available, and a continuum of parameters is needed to describe profiles of temperature, water vapor, and cloud liquid, a rigorous mathematical solution does not exist and the inverse problem is said to be ill-posed [38, 39]. Therefore, it is better to regard the measurements as constraints and to blend them with supplementary sources of information or to drastically reduce the dimensionality of the inverse problem by projecting the profiles onto their linear functionals. Useful supplementary information can be provided by numerical meteorological forecasts, or by a priori information obtained from past data. Examples of profile linear functionals are PWV and LWP for moisture variables and geopotential height for temperature profiles [40]. We briefly discuss algorithms that are commonly used in meteorological remote sensing.

Equation (2a) can be approximated by a Fredholm integral equation of the first kind [9, 40] and in its discrete form is written

$$g_e = Kf + \varepsilon \qquad (5)$$

where g_e is a vector composed of n measurements, f is an m-vector whose components represent the profile that we want to determine, K is an n x m matrix relating the measurements to the unknown profile, and the n-vector ε explicitly denotes that the measurements have an unknown error component that will affect the solution to some degree. For mildly nonlinear problems, the perturbation form expressed by Equation (3) is frequently used as the basis of subsequent iterations. The K matrix is the discrete approximation to the Weighting Functions of Equation (3). If one is working in a spectral region where, for example, humidity, clouds, and pressure contributions to T_b are negligible, then f is a m-vector representing only temperature. In the more general case, f could represent all relevant variables:

$f^T = [(\delta T)^T, (\delta \rho_V)^T, (\delta \rho_L)^T, (\delta P)^T]$ where the superscript denotes matrix transpose. Retrieval algorithms that require calculations of K for their implementation are called "physical." An excellent review article discussing techniques for solving Equation (5) was written by Rodgers [9].

A general algorithm for solving Equation (5) in the linear case is given by

$$\hat{f} - f_0 = [S_f^{-1} + K^T S_\varepsilon^{-1} K]^{-1} \; K^T S_\varepsilon^{-1} (g_e - K f_0) \tag{6}$$

This method is used to incorporate a priori statistics, including means and covariance matrices of f, S_f, and ε, S_ε, into the retrieval process [9, 40]. The matrices S_f and S_ε are defined as $S_f = E\{f - f_0\}\{f - f_0\}^T$ and $S_\varepsilon = E\{\varepsilon\varepsilon^T\}$, where the expectation value E ranges over a joint probability distribution of f and ε. Choices of the function f_0 can include a climatological average, an initial guess based on a forecast, or an estimate derived from another remote sensor, and thus S_f is a measure of the uncertainty in the guess. In some cases, the matrix could be diagonal, with $(\sigma_f)_i^2$ describing the uncertainty at the ith level, or even scalar, with $S_f = (\sigma_f)^2$ were I is the identity matrix. Similarly, S_ε is composed of two terms: the first describes the instrumental uncertainty and the second contains and estimate of the forward model errors. If both S_f and S_ε are scalar, then the ratio $\gamma = (\sigma_\varepsilon)^2 / (\sigma_f)^2$ yields the regularization parameter γ of Twomey [38] and Tikonhov and Arsenin [39]. Iterative extensions of Equation (6) are also discussed by Rodgers [9].

Although Equation (6) is general, and many retrieval methods are its special cases, we mention a few other frequently used methods: neural network inversion [41, 42], Kalman filtering [10, 43, 44, 45], and regression [46]; Kalman Filtering is also a general technique and is described in excellent books [47, 48]. Another technique of great promise is to combine radiometer data with a numerical forecast model, as has been done successfully in satellite meteorology [49, 50].

V. OBSERVATION TECHNIQUES

Measuring downwelling thermal emission by microwave and millimeter wavelength radiometers from a surface-based platform is now routinely performed on an operational basis [2, 3]. In addition, surface-based radiometers are frequently deployed in campaigns specifically designed to study water vapor [35, 36], clouds [51], and temperature [52, 53, 54]. In some deployments, specifically designed to measure water vapor and clouds in combination with other zenith-looking sensors, zenith observations are of primary interest. In others, particularly those used to measure boundary-layer temperature profiles, elevation scanning radiometers are frequently used. More recently, radiometers scanning in both azimuth and elevation are also used to observe clouds [55].

The fundamentals of microwave radiometers are clearly discussed in [13, 56, 57]. Radiometers used to observe the atmosphere are comprised of a highly directional antenna, a sensitive receiver, followed by a detector unit and a data-acquisition system. To produce meteorologically important information, the total system requires calibration. In this section, we briefly discuss general techniques

common to ground-based systems, and then give examples of contemporary radiometers.

V.1. Antennas

An antenna receives the power (as described by Equations (1,2)) that is associated with the antenna temperature, T_A, which is the integration over 4π steradians of the product of the angular distribution of received power and the power pattern of the antenna. Usually, the antennas have symmetric beam patterns with typical widths from 1 to 6°. Because many remote-sensing systems perform scanning in a vertical plane, low side lobes are required to minimize contamination from ground emission. In addition, because surface-based antennas are deployed in rain and snow, protection from and reduction or elimination of environmental effects is of primary concern.

Perhaps the simplest antenna used to observe the atmosphere is a horn, either scalar or corrugated, that has a suitable beam pattern. If a multi-frequency and equal-beamwidth system is desired, the dimensions of the horns can be scaled appropriately. For some systems, the entire electronics package is rotated with the antenna. A more common system is to direct the antenna beam from the primary antenna onto a flat reflecting mirror that is scanned. In this configuration, only the flat reflector is moved. An example of this type of system is shown in Figure 5 [58]. Another common method is to use a lens antenna, which may view a flat reflector. More sophisticated scanning designs are also possible, such as the use of subreflectors, multiple reflectors, and mirrors. Frequently, to protect the system from the environment, the electronics package and the antenna are enclosed within a radome.

It is important to consider the loss from dielectric lens antennas. Lenses for remote sensing are usually constructed from low-loss material (loss tangent less than $\sim 10^{-3}$). A lossy antenna attenuates an incoming signal and adds noise due to its own physical temperature. If the loss factor and the lens temperature are known, the unwanted signal can be corrected from the measured brightness temperature. The effect can be calibrated out by external targets or tipping curves (see Section V.3.2), and a limitation is imposed by the time spent between valid calibration observations.

V.2. Receivers

A variety of receiver designs are also common in surface-based radiometry and several involve Dicke modulation-type radiometers in which the input to the receiver is alternatively switched between the scene (sky) and an internal calibration load [57]. In the original NOAA radiometer [1], the receiver was based on the Hach [59] design in which the signal was sequentially switched between the scene and two internal blackbody targets (hot = 145 °C and reference = 45 °C). These targets were simply waveguide terminations kept at strictly controlled and measured temperatures.
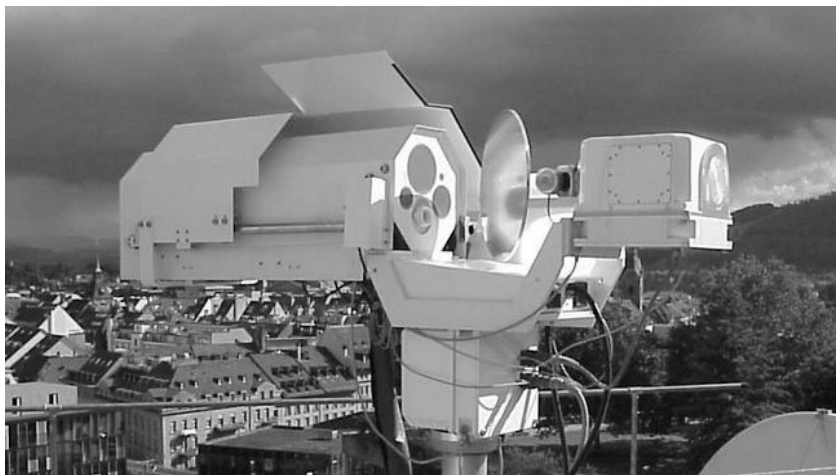
Figure 5 - *ASMUWARA in operation in Bern. The openings of the 4 horns appear as grey disks at the left of the rotatable mirror, while the IR radiometer looks through the white cylinder below the largest horn. The picture also shows on the left the protecting rain roof. During precipitation the rain roof is moved to the right over the mirror. Also visible is the webcam located to the right of the mirror.*

In the Radiometrics Corporation design (http://www.radiometrics.com), a signal generated by a noise diode is alternatively turned off and on and added to the signal from the scene at each angle, including the target [2]. The Russian-designed scanning radiometers for boundary-layer temperature measurement [52, 53, 54] are total-power radiometers but have been modified to include the signal from a noise generator. Both the NOAA Dual Channel radiometer (see Section VI.1) and the NOAA Ground-based Scanning Radiometer (see Section VI.9) receivers use either conventional Dicke or Hach switches that alternate between an internal reference load(s) and the scene. Finally, all of the above receivers are of double-side-band design in which the signal from a stable local oscillator is mixed with the incoming radio-frequency signal emanating from the scene; the intermediate-frequency (IF) signal is then amplified and detected. With IF bandwidths usually around 200 MHz to 1 GHz, 1-sec radiometric sensitivities of 0.1 K are common. Also noteworthy is a specially constructed high-stability radiometer [60]. Based on tipcal analysis (see Section V.3.2), this unit gave rms errors of less than 0.05 K over time periods of a month, and stabilities of better than 0.01 K over time scales of 1000 to 10000 s. Another possibility is to use direct detection at the radio frequency of interest, thus eliminating the mixer and local oscillator. As improvements are made in radio frequency amplifiers, increasing use of direct detection is expected. The use of Dicke or Hach switching overcomes the effect of receiver-gain variations, but reduces the sensitivity of the receiver. As improvements are made in temperature and other environmental controls, total-power radiometers may become more common. Both MICCY (see Section VI.6) and RPG-HATPRO (see Section VI.7) illustrate some of these more recent developments.

V.3. Calibration

To derive quantitative information from radiometric measurements, accurate calibration with accuracies of 0.5 to 1.0 K is required. Most radiometric receivers have one or two internal noise sources that provide some measure of calibration. However, waveguide losses, lack of complete knowledge of radiometric parameters, and a host of other causes usually dictate that some external calibration method also be employed. We assume that the radiometer uses a square law detector, in which the output voltage is proportional to the input power; i. e., voltage is proportional to $B_v(T_A)$. We will briefly describe three commonly used calibration techniques.

V.3.1. External Blackbody Reference Targets

A seemingly straightforward calibration method is to view two external blackbody targets that are kept at two widely separated temperatures [57]. If T_2 and T_1 are the two target temperatures with respective output voltages of v_2 and v_1, then

$$B_v((T_A)_s) = B_v(T_1) + \frac{B_v(T_2) - B_v(T_1)}{v_2 - v_1}(v_S - v_1) \tag{7}$$

where $(T_A)_S$ is the antenna temperature of the scene and v_S is its corresponding voltage. Preferably, the target temperatures bracket the range of antenna temperatures emitted from the scene. Also, it is important to construct targets with high emissivity such that reflections from external sources are negligible, and to have the targets sufficiently large that at least 1½ to 2 projected antenna diameters are captured by the target system. Targets are frequently constructed with a surface having high thermal conductivity covered with a thin layer of very absorbing material. Many times, a corrugated pyramidal surface with wavelength-dependent spacing and depth ratios, is constructed to reduce reflections and hence to increase emissivity. The target is frequently embedded in a thermal insulator that is transparent to incoming radiation. Finally, when a target is placed in a thermal environment in which the environmental temperature differs greatly from desired target temperature, measurements of target temperatures at several locations within the target are essential. The target calibration methods are most useful when the atmospheric brightness temperatures are within the range of easily achieved target temperatures; e.g., near the center of the 60 GHz O_2 absorption or near the 183.31 GHz water vapor line.

V.3.2. The Tipping Curve Calibration Method

In the transmission windows from 20 to 45 GHz or from 70 to 150 GHz, clear-sky T_b's can be in the 10 to 50 K range and, hence, operational deployment of targets whose temperatures are in this range is difficult. In this low transmission case, the so-called tipping-curve calibration method (tipcal) can give a high degree of accuracy [2, 61] and has been commonly used throughout the microwave community. In this method, brightness temperatures are measured as a function of elevation angle θ, and are then converted to opacity $\tau(\theta)$ using the mean radiating

temperature approximation [40]. For each angle θ, an angular-dependent mean radiating temperature $T_{mr}(\theta)$ is used to derive the optical depth $\tau(\theta)$ by

$$\tau(\theta) = \ln\left(\frac{B_\nu(T_{mr}(\theta)) - B_\nu(T_c)}{B_\nu(T_{mr}(\theta)) - B_\nu(T_b(\theta))}\right). \tag{8}$$

We assume in Equation (8) that the antenna temperature $T_A(\theta)$ has been adjusted to $T_b(\theta)$ [61]. If the system is in calibration, then the linear fit of $\tau(\theta)$ as a function of (normalized) air mass m ($= \csc(\theta)$), will pass through the origin; conversely, if $\tau(m) = \tau(1)m + b$ does not pass through the origin, then a single parameter in the radiometer equation is adjusted until it does. Note that when the calibration is achieved, then the slope of the line is equal to the zenith opacity. Several of the factors affecting the accuracy of tipcals were analyzed in [61]. The most serious of these errors are those caused by non-stratified atmospheric conditions and can occur due to clouds and horizontal variations in the water vapor field. Various criteria, based on symmetric scans, are available to determine the quality of a tipcal [2, 61]. In summary, the tipcal method, when applicable, can give absolute accuracies of 0.3 to 0.5 K rms over to 20 to 200 GHz frequency range.

V.3.3. Brightness Temperature Calculations to Calibrate

For a highly stable radiometer such as the NOAA prototype [1] that was operated at a radiosonde launch facility, radiosonde data that are taken during clear-sky conditions can be used with a forward radiative transfer model Equations (2) to calculate T_bs. If the T_bs are taken over a variety of elevation angles, or over a representative range of meteorological conditions, the measured data can be used as calibration points. This method assumes implicitly the correctness of the forward model and also of the radiosondes. The technique is most applicable near highly absorbing spectral regions, such as in the 60 GHz oxygen region, for which the calculated T_bs are insensitive to choice of forward model. When applied to all channels of a multi-frequency radiometer that derives meteorological information, it also ensures internal consistency between radiometric data and the forward model used in retrievals.

V.3.4. Cryogenic Loads to Calibrate

The use of blackbody targets immersed in cyrogenic fluids, such as liquid nitrogen (LN2), is another commonly used method of establishing a single calibration point [63, 64]. In this method, a blackbody target is immersed in the cryogen and the antenna looks directly at the target. Allowance for the reflection of the ambient scene must be made, and the reflection coefficient of the cryogen must also be known. For example, the apparent brightness temperature of LN2 at 290 K at a wavelength of 2.2 mm is 79.05 K [63]. In [64], a series of LN2 calibrations were done, and the Tb differences between the Radiometrics Corporation Microwave Radiometer (see Section VI.2) and the predicted value of Tb emitted from LN2 was within 0.7 K. Frequently a transparent enclosure, such as polystyrene, surrounds the

LN2-immersed blackbody, and care must be taken to avoid condensation on the polystyrene.

I. VI. EXAMPLES OF RADIOMETER SYSTEMS

In this section, we discuss several types of contemporary ground-based radiometers. Since some of these are commercially available, we, of course, do not endorse any particular instrument.

VI.1. NOAA Dual Channel Radiometer

NOAA designed, constructed, and currently operates several dual-frequency radiometers at (20.6 or 23.87 GHz, 31.65 GHz) that are used for measuring PWV and LWP [1]. For each of the radiometers, the electronics, the antenna and the feed are all housed in a benign environment, such as a seatainer (a cargo container that can be deployed either on a ship or on the land). In this enclosed environment, the radiometer is free from precipitation and the internal temperature of the seatainer is controlled to about 5 degrees. The antenna is an offset paraboloid with a hybrid-mode feed, which avoid obstructions of the antenna aperture and results in high-quality radiation patterns that minimize the effect of extraneous sources of noise. The antenna has the same beamwidths at both frequencies (the full width at half power –FWHP– is either 2.5 or 4.0º), thus minimizing differential beam-filling during nonhomogeneous cloud conditions. The parabolic antenna is housed internally in the seatainer and views an external flat reflector through a transparent (mylar) window. By rotating the external reflector, the beam is steerable in a vertical plane. A complete description of the antenna configuration is given in [1]. In addition, some NOAA systems have rapidly rotating reflectors to reduce the effects of rain [65]. The radiometer is triple switched in the Hach [59] mode; this results in continuous internal calibration and high stability. External calibration is accomplished on approximately a weekly basis using the tipcal method in which the external flat reflector is rotated symmetrically through three air masses.

VI.2. Radiometrics Corporation Microwave Radiometer (MWR)

Radiometrics Corporation (http://www.radiometrics.com) has designed, constructed, and delivered several dual-frequency (23.8 and 31.4 GHz) MWRs for measuring PWV and LWP [2]. Each radiometer is easily portable and all electronics, antenna, and calibration targets are enclosed in a radome. The antenna is a corrugated horn with a dielectric lens that views a stepping mirror for scanning the atmosphere and a blackbody target. The FWHP beamwidths of the system are 5.9º at 23.8 GHz and 4.5º at 31.4 GHz. The gain of the system is determined by viewing the target with and without noise injected by a noise diode. Calibration of the system consists in determining the effective noise diode temperature T_{ND} and is done by the tipcal method. When tipcals can't be done, T_{ND} is estimated by an averaging procedure described in [2]. The MWR is equipped with a heated blower and a moisture detector to minimize the effects of rain and dew. Data from several MWR's have been used extensively by the U. S. climate community [62, 87]

VI.3. Tropospheric Water Vapor Radiometer (TROWARA)

At the Institute of Applied Physics (IAP) at the University of Bern, a first generation radiometer system for continuous measurements of PWV and LWP has been operated since 1994. The instrument, called TROWARA, (http://www.iapmw.unibe.ch/research/projects/TROWARA/) was designed and built at the IAP, operating at 21 and 31 GHz [58] with internal calibration (Hach Type [59]), and supplemented by hourly tipping curves [67]. The limitation to two channels requires an estimate of the effective tropospheric temperature [68]. Over the years TROWARA has provided a large data set, which has been used for validating other remote sensing methods [69] and for climate monitoring. The positive PWV bias of 2 mm observed by Ingold and Mätzler [70] over the 1995 to 1998 period was eliminated by radiometer improvements. Since December 2002 the instrument has been working with improved stability and with complete protection against raindrops, thus allowing measurements during all-weather conditions [71].

VI.4. Meteorological Temperature Profiler MTP5

Kipp & Zonen BV is now marketing a radiometer that was originally designed and deployed by the Russian firm ATTEX [52, 54]. This radiometer is designed to measure temperature profiles in the boundary layer from 0 to 600 m above ground level (AGL). The radiometer is a single-channel (61 GHz) solid-state Dicke-type super-heterodyne receiver that is electronically chopped at 1 KHz between the sky and a reference noise source. The antenna is a scalar horn with a FWHP beam width of 6º and scans by viewing a flat reflector at each of 11 scanning angles. Because of the 2 GHz bandwidth and a low receiver noise temperature of 600 K, a high sensitivity of 0.04 K is achieved. Calibration of the receiver is achieved by 0.1°C temperature control and a switched internal noise generator. A one-point absolute calibration is achieved either by viewing an external target or by knowing the emission temperature in the horizontal direction. A variation of this radiometer, developed at NOAA, scans continuously in a 360º vertical plane, and, in addition to temperature profiles, can also be used to measure air-sea temperature difference [53, 72].

VI.5. Radiometrics Corporation Microwave Profiler (MWRP)

Radiometrics Corporation (http://www.radiometrics.com) has also developed a multi-frequency microwave radiometer that is based on a highly stable, tunable, and synthesized, local oscillator in the receiver. This design overcomes errors caused by receiver frequency drift, while allowing observation of a large number of frequencies across wide tuning ranges. The total power receiver has a highly stable noise diode that is used as a gain reference. The radiometer observes atmospheric brightness temperatures in five frequency bands from 22 to 30 GHz, and in seven bands from 51 to 59 GHz [3, 73, 74]. Weighting functions for these bands were shown in Figure 3. It also measures zenith infrared temperature, surface temperature, humidity, and pressure. The radiometer has automated elevation- and azimuth-scanning capability, and the observation interval can be as short as several seconds. The instrument is portable, with 0.12 m^3 volume and 32 kg weight.

VI.6. Microwave Radiometer for Cloud Cartography (MICCY)

MICCY is a 19 frequency 22-channel radiometer that was built by Radiometer Physics GmbH (http://www.radiometer-physics.de) and is operated by the University of Bonn (http://www.meteo.uni-bonn.de) [55] which is capable of high temporal (0.1 s) and spatial (< 1°) resolution. The radiometer has 10 channels on the high-frequency side of the 22.235 GHz water vapor line, 10 channels on the low-frequency side of the 60 GHz O_2 absorption band, and two channels at 90 GHz; at 25.235, 54.8 and 90 GHz both H and V polarization are measured. MICCY is a single sideband total power radiometer that is based on a heterodyne receiver filter-bank design (parallel detection of all frequency channels). The thermal stability of the receivers is less than 20 mK, which implies that the instrument is capable of maintaining its radiometric accuracy for several minutes without recalibration. Both targets and inserted noise from highly stable diodes are used in calibration. With FWHP beam widths of about 0.9º the radiometer is capable of full 360º scanning in azimuth and a zenith scan of 0 to 90º. For mapping of clouds, the entire system can be scanned in azimuth and elevation. The latter is performed by a planar mirror that reflects the incoming radiation into a fixed 1 m Cassegrain system. The system comprises a quasi-optical multiplexer for three frequency bands. Internal ambient and cold blackbodies are used for absolute calibration, while internal noise calibration standards are used in between absolute calibrations. The entire system is mounted on a transportable trailer, and all parts are enclosed in a radome.

VI.7. Radiometer Physics Gmbh-Humidity and Temperature Profiler (RPG-HATPRO)

Because the implementation of an operational network of microwave radiometers is presently hampered by the cost and complexity of available instruments, it was a major objective of the European CLIWA-NET project [51] to develop a network-suitable low-cost microwave radiometer. This radiometer – RPG-HATPRO – has been built by the German company Radiometer Physics GmbH (http://www.radiometer-physics.de). The RPG-HATPRO comprises total-power radiometers utilizing direct detection receivers at all frequencies (14 channels up to 60 GHz). This approach avoids any problems that might arise from mixers or local oscillators (standing waves, frequency drifts, insufficient isolation, sideband suppression, higher system complexity and cost). Thus, the stability and accuracy of the system are drastically improved. Furthermore, possible interferences caused, for example, by communication systems that frequently operate near the IF frequencies, are eliminated. The receivers of each frequency band are designed as filter-banks in order to acquire each frequency channel in parallel. In addition, the flexibility to adjust each channel bandwidth individually allows for optimizing temperature profiling for both boundary layer and full troposphere.

VI.8. All-Sky Multi-Wavelength Radiometer (ASMUWARA)

The ASMUWARA is a radiometer system designed for remote sensing of tropospheric water vapor, cloud liquid water, and temperature profiles (http://www.iapmw.unibe.ch/research/projects/ASMUWARA/) [58]. It was

designed and built at the IAP. The instrument consists of nine microwave channels in the frequency range from 18 to 151 GHz, a broad-band thermal infrared radiometer (wavelength band: 8 to 14 μm), meteorological sensors, including a rain detector, and an optional camera. The radiometers are housed in a temperature-controlled cylinder with all beams aligned in a horizontal direction pointing to a rotating mirror that scans the sky and two calibration loads. The entire instrument can be rotated around its vertical axis. The beams perform a rosetta-like pattern to map the sky hemisphere within 20 minutes. All channels have the same view and a common full beam width of 9°, formed by corrugated horns. The beam width is a compromise between angular resolution and sky coverage within the time scale of atmospheric variations. All horns are vertically polarized. The mirror reflection rotates the polarization during the scan from vertical (at the horizon) to horizontal (at nadir and zenith). A special challenge was to design the optics to cover the broad frequency range, spanning from 18 GHz to the thermal infrared. The solution was to construct a sufficiently large flat aluminum mirror that allowed parallel beams for each spectral range, and to avoid any sort of radome. In this way the instrument works well in periods without precipitation. An extension to all weather operability includes a movable roof with a limited sky view during periods of rain [103]; rain drops on the mirror and calibration load are mostly eliminated. A second IR radiometer, covering the narrower range of 9.6 to 11.5 micrometer, was added to get an additional range indication for clouds. Figure 5 shows the weather-exposed parts of ASMUWARA in operation on the roof at IAP. In principle, ASMUWARA is similar to other recently developed radiometer systems for the troposphere [3, 73, 74]. The main difference is the availability of and the concentration on the hemispheric imaging mode for all channels, including the infrared.

VI.9. NOAA Ground-Based Scanning Radiometer (GSR)

For purposes of Arctic deployments, NOAA designed and constructed a multi-frequency scanning radiometer (http://www.etl.noaa.gov/technology/gsr/) operating from 50 to 380 GHz. The radiometers are installed into a scanning drum or scanhead (see Figures 6). The GSR uses a sub-millimeter scanhead with 11-channels in the 50-56 GHz region, a dual-polarized measurement at 89 GHz, 7-channels around the 183.31 GHz water vapor absorption line, a dual-polarized channel at 340 GHz, and three channels near 380.2 GHz. It also has a 10.6 micrometer infrared radiometer within the same scanhead. All of the radiometers use lens antennas and view two external reference targets during the calibration cycle.
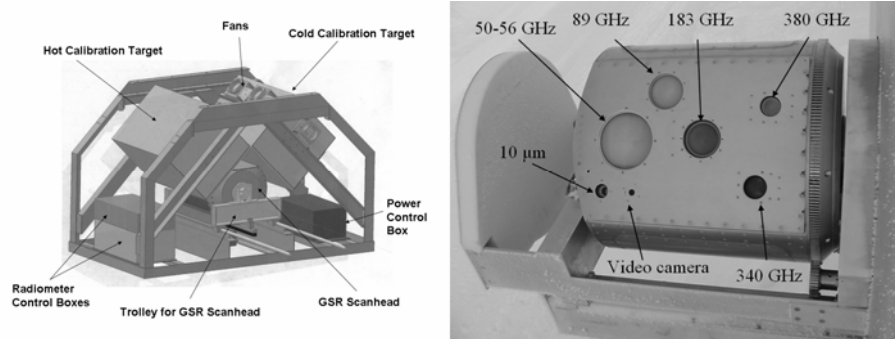
Figure 6 - *Left. Schematic diagram of the GSR calibration and scanning system. The GSR scanhead periodically moves out of the framework for atmospheric viewing on a trolley system, and shares time observing the atmosphere and the two thermally controlled blackbody reference targets. Right. Photograph of the scanhead of the GSR.*

Figure 7 - *Photograph of the deployment of the GSR, MWRP, and MWR at the NSA/AAO Arctic Winter Radiometric Experiment that was conducted in Barrow, Alaska, USA, during March-April 2004.*

In addition, each of the radiometers' design includes two internal reference points for more frequent calibration. The GSR instrument is a modification of a similar instrument that operated at the North Slope of Alaska/Adjacent Arctic Ocean site in 1999 [36]. A substantial improvement in radiometer calibration for ground observation in the Arctic environment has been achieved. Based on experience from the 1999 experiment, a new set of thermally stable calibration targets with high

emission coefficients were also designed, constructed, and deployed. The primary use of the instrument is to measure temperature, water vapor, and clouds, at cold (-20 to -55 °C) and dry (PWV < 5 mm) conditions. A schematic of the GSR is shown in Figure 6. The GSR, along with the MWR and the MWRP, was deployed in the NSA/AAO Arctic Winter Radiometric Experiment that was conducted in Barrow, Alaska, USA, during March-April 2004 [75] (see Figure 7). The beam widths of the GSR channels range from 3.5 to 1.8° and can be averaged to given beam-widths that are consistent with the MWR (4.5° to 5.5°). The GSR performs a scan sequence that includes viewing both the atmosphere and calibration targets. Each scan begins and ends with the radiometer viewing the hot and cold calibration targets. The scanhead then moves out of the calibration housing where it views the atmosphere with a series of continuous and dwell movements. Each scan takes about 2-min to complete. Data from the 26 channels of the GSR should lead to unprecedented information on the evolution of temperature, water vapor, and clouds in the Arctic.

VII. Radiometric Sensing of Tropospheric Meteorological Variables

Remote sensing of meteorological variables by radiometry is now a mature field, with a history of applications at least since the mid 1960's. The strengths of the techniques are accurate calibration, temporal resolutions of the order of seconds, and the ability to measure spatially integrated quantities. In this section, we review a few of the techniques that are now well-established internationally. We then present newer applications that have considerable potential for both research and operational meteorological applications.

VII.1. Integrated Amounts of Water Vapor and Cloud Liquid

Both water vapor and cloud liquid are important variables in meteorology and climate. Due to thermodynamic processes of evaporation and condensation, as well as transport by winds, these quantities vary greatly in space and time. Water vapor is characterized by density as a function of spatial coordinates and time. Water vapor density is limited, depending on temperature, such that the relative humidity is in the range 0 to 100%. To characterize liquid in clouds requires knowledge of particle size as well. Water clouds consist of a large number of droplets of varying sizes. The number of all droplets within a unit volume is the total number density $[m^{-3}]$. The drop size distribution (DSD) describes the number density as a function of droplet radius; i.e., the number of drops per unit volume within a given radius interval. Due to the complex microphysical processes within clouds, DSDs are highly variable in time and space. In contrast to raindrops, cloud droplets are perfect spheres. Thus, all cloud microphysical parameters can be calculated from the DSD. For example, the cloud liquid-water content (LWC) $[kg\ m^{-3}]$ is given by the product of the total volume of water and the density of water. Because the volume of a sphere is proportional to the radius cubed, LWC is also called the third moment of the DSD. It comprises one of the most interesting properties of clouds and is the prognostic variable in most numerical weather prediction and climate models to describe clouds, but few observations are available for the validation of the model results. By

far, the most accurate method to determine the LWP, the vertical integral of LWC, is ground-based passive microwave radiometry. However, for many applications, it is also crucial to know at which altitudes the water is located. To determine the cloud-base height several instruments can be used (e.g. cloud radars, cloud lidar ceilometers, and infrared (IR) radiometers); for cloud thickness, cloud radars are used. Finally, to determine profiles of LWC, the combination of passive microwave and cloud radar measurements is promising [77, 78].

Dual-frequency measurements of brightness temperature at an optimum frequency near the 22.235 GHz water vapor line and in a transmission window have been used to measure PWV and LWP for about 25 years [1, 40, 45]. The general accuracy of dual-frequency radiometric measurement of PWV has been shown to be better than 1 mm rms [35]. However, because of the lack of in situ measurements of cloud liquid, an adequate experimental evaluation of LWP over a range of cloud conditions is not available.

An example of PWV and LWP retrievals is shown in Figure 8. Here, we show the comparisons from data taken during the 2004 NSA/AAO Arctic Winter Radiometric Experiment [75]. Data shown also include surface temperature and infra-red measured cloud base temperature.

Improvements on the dual-channel method can be made with multi-frequency observations. The liquid-water path can be estimated from atmospheric emission measurements in the microwave region because in this spectral region, the cloud contribution strongly increases with frequency (Figures 1 and 2). The standard dual-channel principle has been described above for the determination of PWV. For the retrieval of LWP, the channel close to the water-vapor absorption line corrects for the changing water-vapor concentration of the atmosphere. Such observations are, with the exception of expensive and rather limited aircraft measurements, the most accurate method to observe LWP with an estimated accuracy of better than 25 gm^{-2}. A rough estimation shows that about 10 gm^{-2} are caused by the measurement error while the rest can be attributed to the under-determined retrieval problem. The additional use of the 90 GHz channel can further constrain the problem and improve accuracy to less than 15 gm^{-2} [78].

VII.2. Temperature Profiling by Multi-Frequency Radiometers

Radiometric temperature profiling can be accomplished by measuring the spectrum of radiation intensity at points along the side of the oxygen feature at 60 GHz [79]. By scanning outward from the band center, where the opacity is so great that all signal originates from a distance of some 200-300 m from the antenna, onto the wings of the band, where the radiometer "sees" deeper (higher) into the atmosphere, altitude information is obtained. Emission at any altitude is proportional to local temperature; thus, the temperature profile can be retrieved. Either shoulder of the band center is suitable for retrieval of temperature profile information.
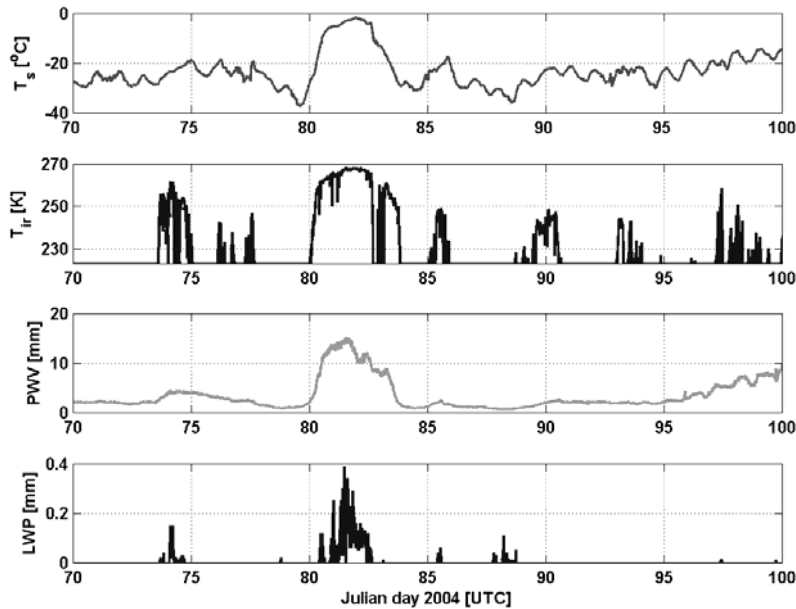
Figure 8 - *Time series of surface temperature (top panel), infra-red measured cloud base temperature, 2nd panel, PWV as measured by the MWRP,3rd panel, and LWP as measured by the MWRP, 4th panel.*

As discussed in Section VI.5, Radiometrics Corporation has developed the MWRP. Historical radiosonde and neural network or regression methods are used for profile retrieval [3] and comparisons between radiosondes and derived profiles are shown in [88]. Retrievals include temperature and humidity soundings up to 10 km height, and one-layer cloud liquid soundings. Radiometric retrievals from this instrument, especially above the boundary layer, have much coarser vertical resolution than radiosonde soundings, but have temporal resolutions of minutes. Retrieval error is smaller than radiosonde sounding error for boundary-layer temperatures, and higher above the boundary layer. The dominant radiosonde error is the representativeness error that results from the characterization of a model cell volume by a point measurement. This type of error is especially important when there are strong temporal or horizontal spatial gradients in the meteorological profiles. Radiometric retrievals can be temporally averaged and, in these strong gradient (temporal or horizontal) conditions may be less susceptible to representativeness error than radiosonde soundings. One of the potential advantages of high-temporal-resolution radiometric data (5 to 15 min) is that the data could be directly assimilated into weather forecast models to improve short term forecasts.

Temperature profiles have also been derived from the ASMUWARA [58]. The temperature profile is retrieved by optimal estimation using Channels 5 through 8 using a climatology from radiosonde data as described in [58, 89, 90]. Temperature profiles of September 18, 2002 are shown in Figure 9. The profiles nicely follow the

temperature development measured at the meteorological station Bantiger on the nearby TV tower. At this early stage, the retrievals of temperature and of atmospheric water are independent. This works well for temperature profiles in the lowest km, where the 57 GHz channel is the dominant source of information

VII.3. Boundary Layer Temperature Profiling from Scanning Radiometers

Angular techniques for measuring emission were developed by NOAA in the early 1970s [80], but due to mechanical simplicity, the zenith-viewing multi-spectral radiometers were chosen by them [1] as a component of a prototype remote-sensing system. However, in 1992, Russian scientists developed a scanning single-channel radiometer that showed promise for routine monitoring of the boundary layer [52, 81]. Development of this kind of radiometer has been continued by the Russian firm (ATTEX) and numerous applications to boundary-layer studies have been published. The technique consists of measuring atmospheric emission at different angles in a wavelength band that exhibits relatively high atmospheric attenuation. The radiometer operates at 60 GHz (wavelength 5 mm), near the peak of the strong oxygen band, has a 6 ° beam width, and can yield data on a 1 sec basis. In this frequency region, the radiation in the horizontal direction can be used as a reference level since T_b is essentially equal to the air temperature at the measurement height. Thus, an accurate air-temperature measurement provides a calibration of the radiometer offset. An independent measurement, such as a laboratory blackbody reference load, or calculations of T_b from radiosondes, is necessary to determine the radiometer's gain. From the downwelling radiation at different elevation angles, atmospheric air temperature profiles can be obtained. As a simple way of explaining the technique, we know that for a constant absorption coefficient, for horizontally stratified atmosphere, and temperature profile that changes linearly with height, the brightness temperature is equal to the air temperature at the position where the opacity is equal to one. For more complex profiles, the optimum retrieval method of Equation (6) must be used. The vertical resolution of the retrieved profiles is a function of altitude, and ranges from about 10 m near the surface to about 300 m at the 500 m altitude. Several experiments were conducted in Russia, Germany, the United Kingdom, and Japan by E. Kadygrov and his co-workers at ATTEX; a similar instrument has been operated by NOAA near Boulder, Colorado, at a meteorological tower [54], at three experiments in Oklahoma, one in the tropics [72], and one at Barrow, Alaska [36]. In all cases, the rms errors were less than 0.5 K below 500 m. An example of temperature measured at 200 m above ground level (AGL) by the radiometer and by in situ measurements on a tower is shown in Figure 10. Because of the simplicity and portability of the instrument and its extremely flexible characteristics, it has been used from airborne, ship-, and ground-based platforms [54, 72, 82].
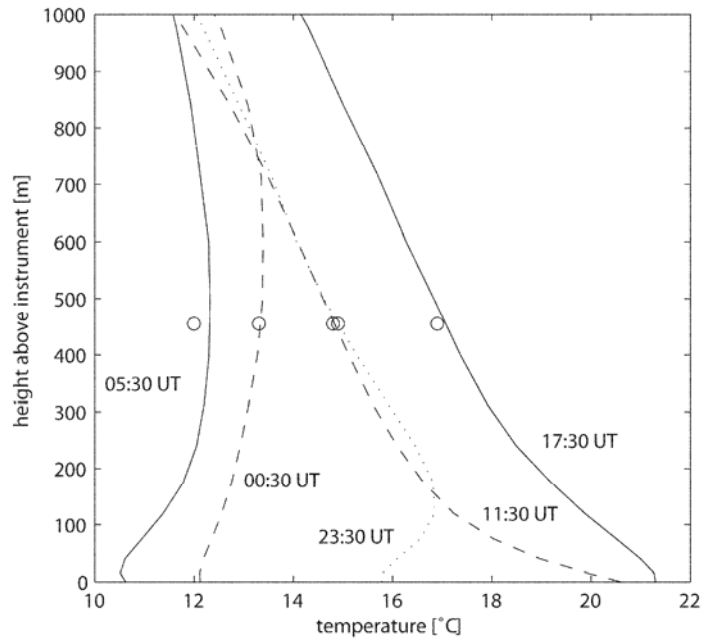
Figure 9 - *Temperature profiles in the lowest km above ground at 5 different times on September 18, 2002 in Bern measured with ASMUWARA and comparison with data from a meteo station (circles) located on a nearby TV tower. After [58].*

VII.4. Angular Scanning Observations of Cloud Liquid

As discussed in Section VI.8, the ASMUWARA is capable of hemispheric imaging of clouds and water vapor. For channels with optically thin radiation, measured T_b can be accurately converted to opacity τ. In turn, equivalent zenith values of IWV and LWP can be derived from τ. Based on local climatology and simulations based on MPM-93 [21], regression coefficients relating τ at 23.6 and 31.4 GHz to IWV and LWP were derived and applied to angular scanning data. A snapshot of the partly cloudy sky is depicted by the LWP data derived from channels 3 and 4 (Figure 11A) and simultaneously by the thermal IR brightness temperature T_{IR} (Figure 11B). Clear sky is represented by LWP = 0 and T_{IR} below −50C. Liquid-water clouds with LWP up to 0.1 kg/m^2 and $T_{IR} \cong$ -25C are apparent. For data evaluation Martin et al. [58] compared PWV values in the range from 2 to 12 kg/m^2 from ASMUWARA with radiosonde data during the first winter period. The radiosonde values were slightly higher (bias 0.8 kg/m^2), whereas the standard deviation was 0.6 kg/m^2.
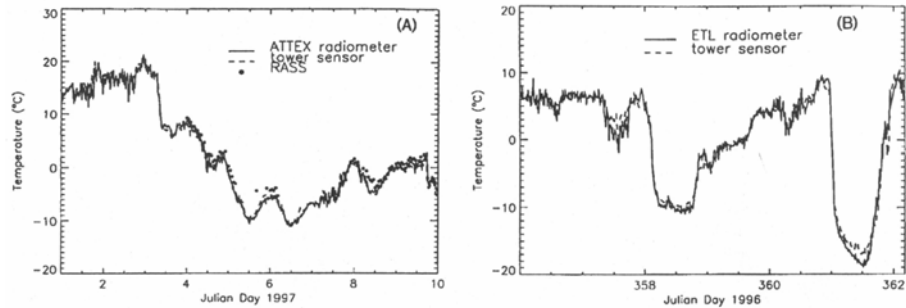
Figure 10 - *(A) A 10-day time series of temperature at 200 m as measured by the ATTEX radiometer, by the in situ measurement on the tower, and by a Radio Acoustic Sounding System (RASS). January 1–10, 1997. (B) A 6-day time series of temperature at 200 m as measured by the NOAA radiometer and by the in situ measurement on the tower. December 21–27, 1996. After [54]*
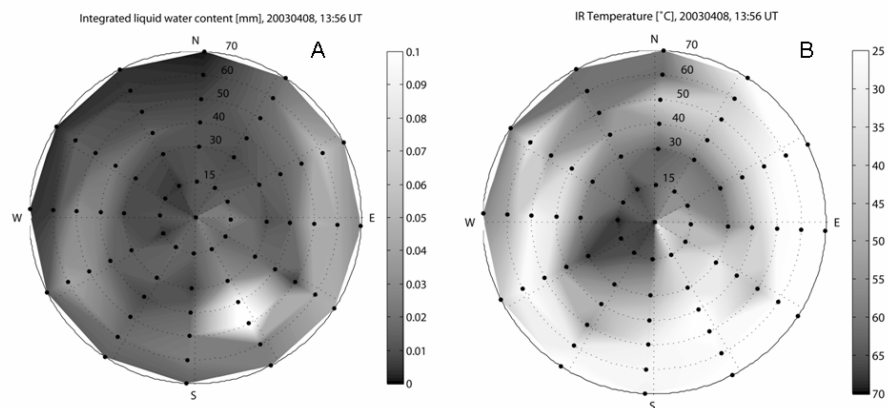

Figure 11 - *(A) Hemispheric Integrated Liquid Water distribution above Bern at 13:56 on April 8, 2003 as derived from ASMUWARA. (B) Hemispheric thermal IR image above Bern at 13:56 on April 8, 2003 as derived from ASMUWARA. After [58].*

While the ASUMUWARA antenna beam width and scan patterns are optimized to provide a fast overview of the entire hemisphere, small scale information on the cloud structure is measured by the microwave radiometer for cloud cartography (MICCY - see Section VI.6) [55]. This radiometer makes scanning measurements with high temporal (0.1 s) and angular (less than 1º) resolution. Figure 12 shows several azimuth scans observed by MICCY, made at an elevation angle of 30°. Scanning measurements improve our estimate of the cloud water distribution and the

cloud structure and such information can be used for studies concerning three-dimensional radiative transfer of solar radiation through clouds.

VII.5. Integrated Profiling by Sensor Synergy

While the cloud water column can be derived accurately from microwave radiometer measurements alone, the information about its vertical distribution is rather limited. Therefore, microwave radiometer measurements are often combined with simultaneous cloud radar observations which provide the radar reflectivity factor Z with a vertical resolution of approx. 50-100 m. Since Z is proportional to the sixth moment of the drop size distribution and the cloud liquid water content LWC is proportional to the third, a direct conversion of Z to LWC results in large errors. Thus, a common approach used by Frisch et al. [92] scales the radar reflectivity profile to the LWP as measured by a radiometer. A more sophisticated, physically based technique [93] combines the microwave brightness temperatures, the attenuation-corrected radar reflectivity profile, the lidar-ceilometer cloud base, ground temperature and humidity, and the nearest operational radiosonde profile within an optimal estimation retrieval. This Integrated Profiling Technique (IPT) can simultaneously derive profiles of temperature, humidity, and LWC. The retrieved IPT profiles are characterized by their physical consistency with respect to the microwave radiometer and cloud radar measurements. Additional constraints guarantee a match with the ground-level measurements, saturation within the cloud boundaries, and statistical consistency with the radiosonde temperature and humidity profiles.

Error covariances of all measurements are required, such that all constraints can be met within an iterative optimal estimation procedure. The solution is interpreted as a probability density so that a retrieval error estimate is inherently given. A further advantage of the IPT is that, in contrast to the LWP scaling methods, the LWC profiles are independent of errors of an LWP algorithm.

Presently, the IPT has been developed only for cases when the radar reflectivity is solely caused by liquid-water drops. This means that the occurrence of mixed phase clouds within the vertical column above the instruments will make IPT application impossible. However, the presence of pure ice clouds above one or more liquid cloud layers will not influence the IPT because ice clouds do not contribute to the microwave signal in the frequency range below 90 GHz. Furthermore, insect- and precipitation-dominated radar pixels need to be removed. Thus, to be able to apply the IPT automatically, a cloud classification was developed that distinguishes between six phases/regimes (pure ice, mixed-phase, pure liquid water, drizzle, significant precipitation and unclassified). The classification makes use of cloud radar, lidar-ceilometer, the nearest operational radiosonde temperature profiles, and microwave-radiometer-derived LWP. An example of the cloud classification for one day is shown in Figure 13. Obviously, the ice- and mixed-phase- clouds dominate the radar signal. Although the classification suggests that water clouds play a minor role, their strong influence on the solar radiation makes them of utmost importance for climate research.
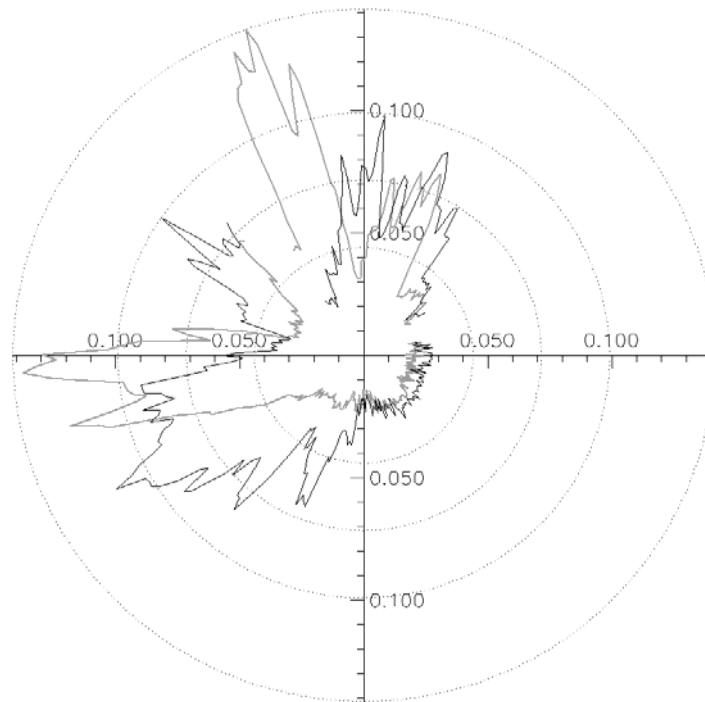
Figure 12 - *Series of 14 successive azimuth scans at 30 deg elevation with the multi-channel microwave radiometer MICCY having a beam width of less than 1 deg in all channels. Liquid water path was derived using a regression algorithm employing four frequency channels. After [55].*

The advantage of microwave remote sensing is that even in the presence of thick clouds, temperature and humidity can be determined with good accuracy. However, because the vertical resolution is relatively coarse (about 1-2 km [88]) sharp inversions can't be resolved completely.

The IPT is a first step toward an "all-encompassing" profiling algorithm which combines measurements from all available instruments to derive the atmospheric state as accurately as possible. Since this task should ideally be accomplished in a physically consistent way, knowledge of all involved forward models is required. Future extensions will include infrared and ceilometer forward models to further constrain cloud microphysical parameters, especially in the lower part of the cloud.
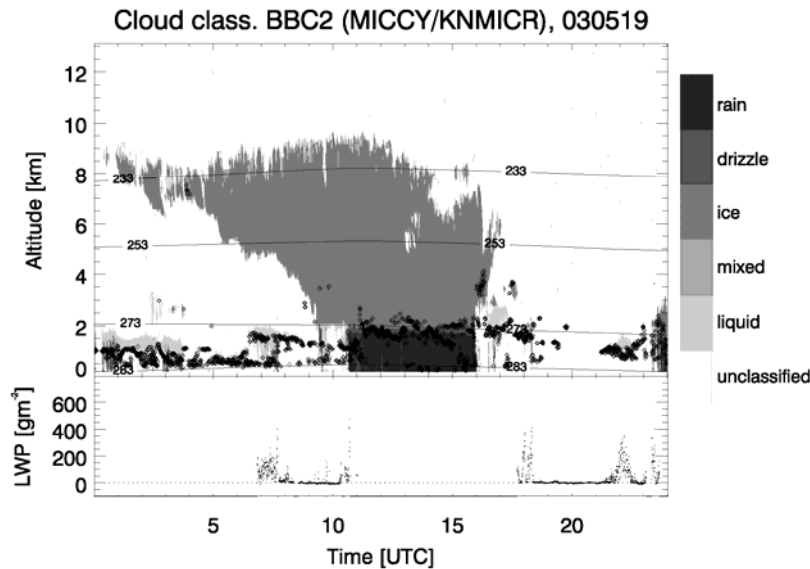
Figure 13 - *Cloud classification and LWP for May 19, 2003 at Cabauw. Temperature is derived from interpolated radiosondes. The classification is performed for each individual cloud radar range gate. Black dots indicate the cloud base height as observed by lidar ceilometer.*

VII.6. Climate Applications

In the United States, the Department of Energy's Atmospheric Radiation Measurement (ARM) has developed a long-range program to study the effects of clouds on climate and on the development of climate models [87, 91]. In their experimental facilities to measure clouds and radiation, the ARM program has developed and operates three research sites in the Southern Great Plains (SGP), in North Central Oklahoma, USA, on the North Slope of Alaska (NSA), and in the tropical western Pacific (TWP). Because of their proven ability to measure PWV and LWP, ARM has deployed 10 MWRs (see Section VI.2) at their various research sites [2, 87]. The ARM facilities also routinely launch radiosondes, and operate infrared and optical radiation sensors, lidars, and Millimeter Wave Cloud Radars (MMCR). In addition to providing measurement tools valuable for climate research, many of the data can be used to develop combined-sensor meteorological products.

One of the important results of MWR deployment has been the discovery and correction of dry bias humidity errors in Väisäla RS80 humidity sensors [7, 62]. The errors were first discovered in the comparison of measurements and radiosonde-based calculations of infrared radiance; consequently, three Water Vapor Intensive Operating Periods (WVIOPs) were conducted at the SGP [35] to address the problem. Several MWRs from a variety of US research institutions were deployed, and many kinds of radiosonde intercomparisons were also done. As a result of these WVIOPs, all radiosondes launched at the SGP site were scaled by MWR PWV

measurements. An example of the need for radiosonde corrections is shown in Figure 14, in which comparisons of calculations and MWR measurements are given. In this case, the use of an uncorrected radiosonde gave rise to a calculation error of about 10 K. Radiosonde data for this experiment were taken at the Atmospheric Radiation and Cloud Station ARCS at the Republic of Nauru [62].

The MWR retrievals of LWP are also useful in developing models to calculate the transfer of solar radiation through clouds containing liquid, including mixed-phase clouds. In particular, when MMCR and MWR are both available, the information on particle size distribution can also be derived [92]. It is apparent that for years to come, the MWR will provide useful data for studying radiative transfer through clouds.

VIII. CONCLUDING REMARKS

For the past 35 years, surface-based microwave radiometers operating below 60 GHz have provided useful data on temperature, water vapor, and clouds. Steady progress has been made in the development of robust, sensitive, and accurate radiometers. This has been accompanied by continued development of forward models for the accurate calculation of brightness temperature, although there is still some concern about cloud liquid characterization below freezing temperatures. The development of suitable inverse models has also occurred, but, it now seems likely that assimilation of data with forecast models is the most promising technique for exploiting radiometer data [76, 98]. Of equal promise, is the synergism of active and passive sensors, as has been achieved in cloud sensing [77, 78], in moisture profiling [94, 95, 96], and in the use of wind profiler estimates of significant moisture gradients to improve humidity profile retrieval [95].

Another promising area of research is the development of scanning radiometers that can measure horizontal gradients in water vapor and cloud liquid. For example, moisture gradients are frequently seen in tipcal measurements by MWRs [61]. The ASMUWARA has the potential to be an important tool for ground-based remote sensing of the troposphere. Advancements are expected to be made from the participation at the COST-720 intercomparison campaign for temperature, humidity and cloud profiling that was made in Payerne (Switzerland) from November 2003 to January 2004 [99-105]. Improvements will include the synergy of all channels in a coherent retrieval. With respect to instrumentation of ASMUWARA, an advancement was the addition of a 151 GHz channel, which allows higher sensitivity to clouds. Also to be exploited is the potential to measure precipitation [97]; for this purpose use will be made of the lower frequency channels in case of rain and the 151 GHz channel for dry snow. If the methods are successful, ASMUWARA will become a valuable tool in the ground validation of the international Global Precipitation Mission to be created by the space agencies of Europe, Japan and the USA.
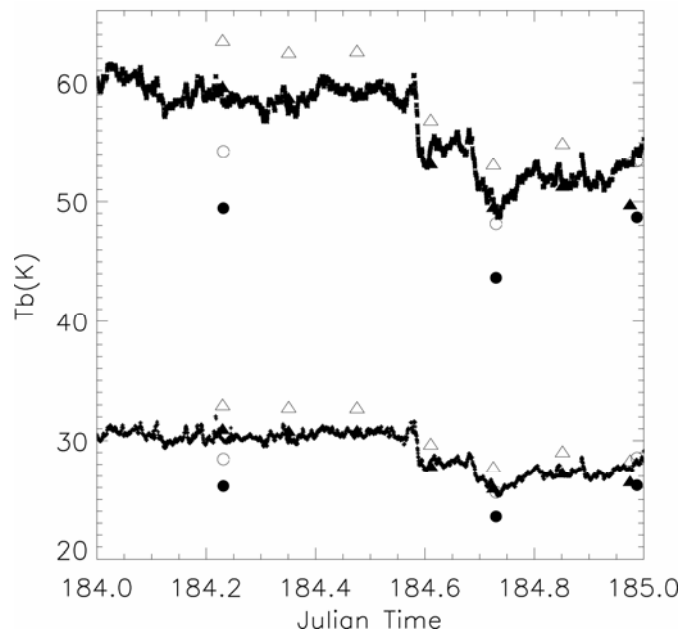
Figure 14 - *24-hr time series of Tb at 23.8 (*) and 31.4 GHz (+) on 3 July, 1999. Closed circles — calculated from original ARCS-2 radiosondes (age = 315 days). Open circles — calculated from corrected ARCS-2 radiosondes. Closed triangles — calculated from original RHB radiosondes (age = 172 days). Open triangles — calculated from corrected RHB radiosondes. RTE model [5]. After [62].*

Finally, the sensitivity of radiometers to both water vapor and cloud liquid increases with frequency, and arctic regions, with typical small amounts of both liquid and vapor, seem especially amenable to millimeter wave radiometry. As satellite sensors increasingly use millimeter wavelength radiometers, accurate forward models for satellite retrievals can be developed by using data from upward-looking sensors coupled with radiosondes. Such forward models are important in surface-, airborne-, and satellite-based remote sensing, as well as for communication.

ACKNOWLEDGEMENTS

References

[1]   D. C. Hogg, M. T. Decker, F. O. Guiraud, K. B. Earnshaw, D. A. Merritt, K. P. Moran, W. B. Sweezy, R. G. Strauch, E. R. Westwater, and C. G. Little, "An Automatic Profiler of the Temperature, Wind and Humidity in the Troposphere," *Journal of Applied Meteorology*, **22**, 5, 1983, pp. 807-831.

[2]   J. C. Liljegren, "Automatic Self-Calibration Of ARM Microwave Radiometers," in P. Pampaloni and S. Paloscia, (eds.), *Microwave Radiometry and Remote Sensing of the Earth's Surface and Atmosphere*, Utrecht, VSP Press, 2000, pp. 433-441.

[3]   R. Ware, R. Carpenter, J. Güldner, J. Liljegren, T. Nehrkorn, F. Solheim, and F. Vandenberghe, "A Multi-Channel Radiometric Profiler of Temperature, Humidity and Cloud Liquid," *Radio Science*, **38**, 4, 2003, pp. 8079-8032.

[4]   H. J. Liebe, "MPM, An Atmospheric Millimeter Wave Propagation Model," *International Journal of Infrared and Millimeter Waves*, **10**, 6, 1989, pp. 631-650.

[5]   . P. W. Rosenkranz, "Water Vapor Microwave Continuum Absorption: A Comparison of Measurements and Models," *Radio Science,* **33,** 4, 1998, pp. 919-928.

[6]   P. W. Rosenkranz, Correction to "Water Vapor Microwave Continuum Absorption: a Comparison of Measurements And Models, *Radio Science*, **34**, 4, 1999, pp. 1025.

[7]   H. J. Liebe, G. A. Hufford, and T. Manabe, "A Model for the Complex Permittivity of Water at Frequencies below 1 THz," *International Journal of Infrared and Millimeter Waves*, **12**, 7, 1991, pp. 659-675.

[8]   D. Turner, B. Lesht, A. Clough, J. Liljegren, H. Revercomb, and D. Tobin, "Dry Bias and Variability in Väisälä RS80-H Radiosondes: The ARM Experience," *Journal of Atmospheric and Oceanic Technology,* **20**, 1, 2003, pp.117-132.

[9]   E. E. Clothiaux, T. P. Ackerman, G. G. Mace, K. P. Moran, R. T. Marchand, M. A. Miller, and B. E. Martner,: "Objective Determination of Cloud Heights and Radar Reflectivities Using a Combination of Active Remote Sensors at the ARM CART Sites," *Journal of Applied Meteorology*, **39,** 5, 2000, pp. 645–665.

[10] C. D. Rodgers, "Retrieval of Atmospheric Temperature and Composition From Remote Measurements of Thermal Radiation," *Reviews of Geophysics and Space Physics,* **14**, 1976, pp.609-624.

[11] Y. Han, E. R. Westwater, and R. A. Ferrare, "Applications of Kalman Filtering to Derive Water Vapor from Raman Lidar and Microwave

Radiometers," *Journal of Atmospheric and Oceanic Technology*, **14**, 3, 1997, pp. 480-487.

[12] E. R. Westwater, S. Crewell, C. Matzler, "A Review of Surface-based Microwave and Millimeter wave Radiometric Remote Sensing of the Troposphere", *Radio Science Bulletin of URSI*, RSB-310. September 2004, **59-80**, ISSN 1024-4530.

[13] R. M. Goody and Y. L. Yung , "Atmospheric Radiation", *Theoretical Basis, Oxford University Press*, Second Edition, 1995, 544 pages.

[14] M. A. Janssen, "An Introduction to the Passive Remote Sensing of Atmospheres," in Michael A. Janssen (ed.), *Atmospheric Remote Sensing by Microwave Radiometry*, New York, J. Wiley & Sons, Inc, 1993, pp.1-36.

[15] A. J. Gasiewski, "Microwave Radiative Transfer in Hydrometeors," in Michael A. Janssen (ed.), *Atmospheric Remote Sensing by Microwave Radiometry*, New York, J. Wiley & Sons, Inc., 1993, pp. 91-144.

[16] M. Klein and A. J. Gasiewski, "Nadir Sensitivity of Passive Millimeter and Submillimeter Wave Channels to Clear Air Temperature and Water Vapor Variations," *Journal of Geophysical Research,* **105,** D13*, 2000, pp. 17481-17511.

[17] J. H. van Vleck, "The Absorption of Microwaves by Uncondensed Water Vapor", *Physical Review ,*71, 425–433 (1947).

[18] J. H. van Vleck, "The Absorption of Microwaves by Oxygen", *Physical Review,*71, 413–424 (1947)

[19] J. H. van Vleck and V. F. Weisskopf, "On the Shape of Collision Broadened Lines", *Reviews of Modern Physics,***17,** 227-236 (1947).

[20] P. W. Rosenkranz, "Absorption Of Microwaves By Atmospheric Gases," Chapter 2 in Michael A. Janssen (ed.), *Atmospheric Remote Sensing by Microwave Radiometry*, M. A. Janssen, Ed., New York, J. Wiley & Sons, Inc., 1993, pp. 37-90.

[21] H. J. Liebe and D. H. Layton, "Millimeter Wave Properties of the Atmosphere: Laboratory Studies and Propagation Modeling," National Telecommunications and Information Administration (NTIA) Report 87-24, 1987, 74 pp. (available from the National Technical Information Service, 5285 Port Royal Road, Springfield, VA, 22161).

[22] H. J. Liebe, G. A. Hufford, and M. G. Cotton, "Propagation Modeling of Moist Air and Suspended Water/Ice Particles at Frequencies below 1000," in *AGARD Conference Proceedings 542, Atmospheric propagation effects through natural and man-made obscurants for visible through MM-wave radiation*, 1993, pp. 3.1 to 3.10 (available from NASA Center for Aerospace Information, Linthicum Heights, MD).

[23] P. W. Rosenkranz, Massachusetts Institute of Technology, Cambridge, MA, private communication, March 2004.

[24] J. C. Liljegren, S. A. Boukabara, K. Cady-Pereiria, and S. A. Clough, "The Effect of the Half-Width of the 22-GHz Water Vapor Line on Retrievals of Temperature and Water Vapor Profiles with a Twelve-Channel Microwave Radiometer," *IEEE Transactions on Geoscience and Remote* Sensing, **43**(5), pp. 1102-1108, 2005.

[25] V. Mattioli, E. R. Westwater, S. I. Gutman, and V. R. Morris, "Forward Model Studies of Water Vapor using Scanning Microwave Radiometers, Global Positioning System, and Radiosondes during the Cloudiness Inter-Comparison Experiment", *IEEE Transactions on Geoscience and Remote Sensing,*. **43**(5), pp. 1012-1021, 2005.

[26] H. C. Van de Hulst, *Light Scattering by Small Particles*, New York, Dover Publications Inc.,1981.

[27] D. Deirmendjian, *Electromagnetic Scattering on Spherical Polydispersions*, New York, American Elsevier Publishing Company, Inc., 1969.

[28] C. F. Bohren and D.R. Huffman, *Absorption and Scattering of Light by Small Particles*, New York, John Wiley, 1983.

[29] P. Debye, *Polar Molecules*, New York, Dover, 1929.

[30] E. H. Grant, J. Buchanan, and H. F. Cook, "Dielectric Behavior of Water at Microwave Frequencies," *Journal of Chemical Physics,* **26**, 1957, pp. 156-161.

[31] V. I. Rosenberg, *Scattering and Extinction of Electromagnetic Radiation by Atmospheric Particles*, Leningrad, Gidrometeoizdat, (in Russian), 1972.

[32] E. R. Westwater, Y. Han, M. D. Shupe, and S. Y.Matrosov, "Analysis of Integrated Cloud Liquid and Precipitable Water Vapor Retrievals from Microwave Radiometers during SHEBA," *Journal of Geophysical Research*, **106**, 23, 2001, pp. 32019-32030.

[33] R. Rasmussen et al., "Winter Icing and Storms Project (WISP)," *Bulletin of the American Meteorological Society*, **73**, 7, 1992, pp. 951-974.

[34] G. Hufford, "A Model for the Complex Permittivity of Ice at Frequencies below 1 THz," *International Journal of Infrared and Millimeter Waves*, **12**, 1991, pp. 677-682.

[35] C. Mätzler, "Microwave Properties of Ice and Snow," in B. Schmitt et al. (eds.), *Solar System Ices, Astrophysica, and Space Science Library,* **227**, Dordrecht, Kluwer Academic Publishers, 1998, pp. 241-257.

[36] H. E. Revercomb et al., "The ARM Programs's Water Vapor Intensive Observation Periods: Overview, Initial Accomplishments, and Future

Challenges," *Bulletin of the American Meteorological Society*, **84**,1, 2003, pp. 217-236

[37] P. E. Racette et al., "Measurement of Low Amounts of Precipitable Water Vapor Using Ground-Based Millimeterwave Radiometry," J*ournal of Atmospheric and Oceanic Technology*, **22(4)**, pp. 317 - 337, April 2005.

[38] E. R. Westwater, S. Crewell, and C. Matzler, "Surface-based Microwave and Millimeter wave Radiometric Remote Sensing of the Troposphere: a Tutorial", *IEEE Geoscience and Remote Sensing Newsletter*, March 2005, **16-33**. ISSN 0161-7869.

[39] S. Twomey, *Introduction to the Mathematics of Inversion in Remote Sensing and Indirect Measurements*, New York, Elsevier, 1977.

[40] A. N. Tikhonov and V. Y. Arsenin, *Solutions of Ill-Posed Problems*. Washington, DC, V.H. Winston and Sons, 1977.

[41] E. R. Westwater, "Ground-based Microwave Remote Sensing of Meteorological Variables," in Michael A. Janssen (ed.), *Atmospheric Remote Sensing by Microwave Radiometry*, New York, J. Wiley & Sons, Inc., 1993, pp. 145-213.

[42] J. H. Churnside, J. H., T. A. Stermitz, and J. A. Schroeder, "Temperature Profiling with Neural Network Inversion of Microwave Radiometer Data," *Journal of Atmospheric and Oceanic Technology,* **11**, 1994, pp.105-109.

[43] F. Del Frate and G. Schiavon, "A Combined Natural Orthogonal Functions/Neural Network Technique for Radiometric Estimation of Atmospheric Profiles," *Radio Science*, **33**, 1998, pp. 405-410.

[44] W. M. Ledskam and D. H. Staelin, "An Extended Kalman-Bucy Filter for Atmospheric Temperature Profile Retrieval with a Passive Microwave Sounder," *Journal of Applied Meteorology*, **17,** 1978, pp. 1023-1033.

[45] H. E. Moteller, L. L. Strow, and L. McMillin, and J. A. Gualtieri, "Comparison of Neural Networks and Regression-Based Methods for Temperature Retrievals," *Applied Optics*, **34**, 1995, pp. 5390-5397.

[46] J. Askne and E.R. Westwater, "A Review of Ground-Based Remote Sensing of Temperature and Moisture by Passive Microwave Radiometers," *IEEE Transactions on Geoscience And Remote Sensing*, **G3-24**, 1986, pp. 340-352.

[47] N. A. Phillips, L. M. McMillin, D. Wark, and A. Gruber, "An Evaluation of Early Operational Temperature Soundings from TIROS-N," *Bulletin of the American Meteorological Society*, **60**, 1979, pp. 1188-1197.

[48] A. Gelb, *Applied Optimal Estimation*, Cambridge, MA, The M. I. T. Press, 1988.

[49] R. G. Brown and P. Y. C. Hwang, *Introduction to Random Signals and Applied Kalman Filtering*, New York, J. Wiley & Sons, 1997.

[50] J. C. Derber and W.-S. Wu, "The Use Of TOVS Cloud-Cleared Radiances in the NCEP SSI Analysis System," *Monthly Weather Review*, **126**, 1998, pp. 2287-2302.

[51] G. Ohring, K. Michell, M. Ji, S. Lord, and J. Derber, "Applications of Satellite Remote Sensing in Numerical Weather and Climate Prediction," *Advances in Space Research* **30**, 2002, pp. 2433-2439.

[52] S. Crewell, M. Drusch, E. van Meijgaard, and A. van Lammeren, "Cloud Observations and Modeling within the European BALTEX Cloud Liquid Water Network," *Boreal Environmental Research,* **7**, 2002, pp. 235-245.

[53] E. N. Kadygrov and D. R. Pick, "The Potential Performance of an Angular Scanning Single Channel Microwave Radiometer and some Comparisons with in Situ Observations," *Meteorological Applications, UK*, **5**, 1998, pp. 393-404.

[54] Yu. G. Trokhimovski, E. R. Westwater, Y. Han, and V. Ye. Leuskiy, "The Results of Air and Sea Surface Temperature Measurements using a 60 Ghz Microwave Rotating Radiometer," *IEEE Transactions on Geoscience And Remote Sensing*, **36**, 1, 1998, pp. 3-15.

[55] E. R. Westwater, Y. Han, V. G. Irisov, V. Leuskiy, E. N. Kadygrov, and S. A. Viazankin, "Remote Sensing of Boundary-Layer Temperature Profiles by a Scanning 5-mm Microwave Radiometer and RASS: Comparison Experiment," *Journal of Atmospheric and Oceanic Technology*, **16**, 7, 1999, pp. 805-818.

[56] S. Crewell, H. Czekala, U. Löhnert, C. Simmer, Th. Rose, R. Zimmermann, and R. Zimmermann, "Microwave Radiometer for Cloud Carthography: A 22-Channel Ground-Based Microwave Radiometer for Atmospheric Research," *Radio Science*, **36**, 2001, pp. 621-638.

[57] F. T. Ulaby, R. K. Moore, and A. K. Fung, *Microwave Remote Sensing, Active and Passive. Volume 1, Microwave Remote Sensing Fundamentals and Radiometry*, Reading, MA, Addison-Wesley Publishing Company, 1981.

[58] N. Skou, *Microwave Radiometer Systems: Design and Analysis*, Norwood, MA, Artech House, Inc., 1989.

[59] L. Martin, A. Lüdi and C. Mätzler, "Tropospheric Monitoring with ASMUWARA", Proc. 6th International Symposium on Tropospheric Profiling (ISTP): Needs and Technologies, Leipzig, Germany, Sep. 14-20, 2003.

[60] J. Hach, "A Very Sensitive Airborne Radiometer using Two Reference Temperatures," *IEEE Transactions on Microwave Theory and Techniques*, **MTT-16**, 9, 1968, pp. 629-636.

[61] A. B. Tanner and A. L. Riley, "Design and Performance of a High-Stability Water Vapor Radiometer," *Radio Science*, **38** , 3, 2003, 8050, doi:10.1029/2002RS002673.

[62] Y. Han and E. R. Westwater, "Analysis and Improvement of Tipping Calibration for Ground-Based Microwave Radiometers," *IEEE Transactions on Geoscience and Remote Sensing*, **38**, 2003, pp. 1260-1277.

[63] E. R. Westwater, B. B. Stankov, D. Cimini, Y. Han, J. A. Shaw, B. M. Lesht, and C. N.Long, "Radiosonde Humidity Soundings and Microwave Radiometers during Nauru99 *Journal of Atmospheric Oceanic Technology*, **20**, 7,2003, pp. 953-971.

[64] A. McGrath and T. Hewison**, "**Measuring the Accuracy of MARSS—An Airborne Microwave Radiometer**,***" Journal of Atmospheric and Oceanic Technology,* **18***, 2001*, pp. 2003–2012*.

[65] D. Cimini, E. R. Westwater, Y. Han, S. J. Keihm. "Accuracy of ground-based microwave radiometer and balloon-borne measurements during the WVIOP2000 field experiment," *IEEE Transactions on Geoscience and Remote Sensing*, **41,** 11**,** 2003, pp**.** 2605-2615.

[66] M. D. Jacobson and W.M. Nunnelee, "Design and Performance of a Spinning Flat Reflector for Millimeter-Wave Radiometry," *IEEE Transactions on Geoscience and Remote Sensing*, **35**, 1997, pp. 464-466.

[67] R. Peter and N. Kämpfer, "Radiometric Determination of Water Vapor and Liquid Water and its Validation with other Techniques," *Radio Science,* **97** ,D16, 1992, pp. 18173-18183.

[68] C. Mätzler. "Ground-Based Observations of Atmospheric Radiation at 5, 10, 21, 35 And 94 GHz," *Radio Science*, **27**, 1992, pp. 403-415.

[69] T. Ingold, R. Peter, and N. Kämpfer, "Weighted Mean Tropospheric Temperature and Transmittance Determination at Millimeter-Wave Frequencies for Ground-Based Applications," *Radio Science*, **33**, 1998, pp. 905-918.

[70] T. Ingold, B. Schmid, C. Mätzler, P. Demoulin and N. Kämpfer, "Modeled and Empirical Approaches for Retrieving Columnar Water Vapor from Solar Transmittance Measurements in the 0.72, 0.82 and 0.94 μm Absorption Bands", *Journal of Geophysical Research*, **105(D19)**, 2000, pp. 24327-24343.

[71] T. Ingold and C. Mätzler, "Four Years of Columnar Water Vapor Measurements Above the Swiss Central Plain Using Radiosondes and a Microwave Radiometer", IAP Research Report No. 2000-02, Institute of applied Physics, University of Bern, Bern, Switzerland, April (2000).

[72] J. Morland, "TROWARA – Tropospheric water vapour radiometer: Radiometer review and new calibration model", IAP Res. Rep. 2002-15,

Institute of applied Physics, University of Bern, Bern, Switzerland, November (2002).

[73] D. Cimini, J. A. Shaw, Y. Han, E. R. Westwater, V. Irisov, V. Leuski, and J. H. Churnside, "Air Temperature Profile and Air-Sea Temperature Difference Measurements by Infrared and Microwave Scanning Radiometers," *Radio Science*, **38**, 3, 8045, doi:10.1029/2002RS002632, 2003.

[74] F. Solheim, J. Godwin, E. Westwater, Y. Han, S. Keihm, K. Marsh, R. Ware, "Radiometric Profiling of Temperature, Water Vapor, and Liquid Water using Various Inversion Methods," *Radio Science*, **33**, 1998, pp. 393-404.

[75] J. C. Liljegren, "Improved Retrievals of Temperature and Water Vapor Profiles with a Twelve-Channel Radiometer," in *2004 Proc. of the Eighth Symposium on IOAS-AOLS*, American Meteorological Society, 11-15 Jan. 2004, Seattle, WA.

[76] E. R. Westwater et al.,"Initial Results from the 2004 North Slope of Alaska Arctic Winter Radiometric Experiment", Proc. IGARSS'04, Anchorage, AK, USA, Sept. 20-24, 2004.

[77] G. Ohring, K. Michell, M. Ji, S. Lord, and J. Derber, "Applications of Satellite Remote Sensing in Numerical Weather and Climate Prediction," *Advances in Space Research* **30**, 2002, pp. 2433-2439.

[78] U. Löhnert, S. Crewell, A. Macke, and C. Simmer, "Profiling Cloud Liquid Water by Combining Active And Passive Microwave Measurements with Cloud Model Statistics," *Journal of Atmospheric and Oceanic Technology*, **18**, 2001, pp. 1354-1366.

[79] S. Crewell and U. Löhnert, "Accuracy Of Cloud Liquid Water Path from Ground-Based Microwave Radiometry. Part II. Sensor Accuracy and Synergy," *Radio Science*, 38(3), 2003, 8042, doi:10.1029/2002RS002634.

[80] E. R. Westwater, "Ground-based Passive Probing Using the Microwave Spectrum of Oxygen,": *Radio Science Journal of Research of the NBS,* **9D**, 9, 1965, pp. 1201-1211

[81] E. R. Westwater, J.B. Snider, and A.C. Carlson, "Experimental Determination of Temperature Profiles by Ground-Based Microwave Radiometry," *Journal of Applied Meteorology*. **14,** 4, 1975, pp. 524-539.

[82] K. P. Gaikovich, E. N. Kadygrov, A. S Kosov, A. V. Troitskiy, "Thermal Sounding of the Boundary Layer of the Atmosphere at the Center of the Line of Oxygen Absorption," *Izvestia vuzov, Radiophysica,* **35**, 2, 1992, pp. 130-136.

[83] V. Leuskii, V. Irisov, E. Westwater, L. Fedor, and B. Patten, "Airborne measurements of the sea-air temperature difference by a scanning 5-mm

wavelength radiometer," Proc. IGARSS2000, pp. 260-262, July 24-28, Honolulu, Hawaii, USA, 2000.

[84] S. A. Clough, M.W. Shephard, E.J. Mlawer, J.S. Delamere, M.J. Iacono, K. Cady-Pereira, S. Boukabara, and P.D. Brown. 2005. "Atmospheric radiative transfer modeling: a summary of the AER codes." *Journal of Quantitive Spectroscopy and Radiative Transfer*, 9, 233-244.

[85] M. Yu. Tretyakov, M. A. Koshelev, V. V. Dorovskikh, D. S. Makarov, and P. W. Rosenkranz, "60-GHz oxygen band: precise broadening and central frequencies of fine-structure, absolute absorption profile at atmospheric pressure, and revision of mixing coefficients," *Journal of Molecular Spectroscopy*, **231**, 2005, pp. 1-14.

[86] M. Yu. Tretyakov, V. V. Parshin, M. A. Koshelev, V. N. Shanin, S. E. Myasnikova, and A. F. Krupnov, "Studies of 183 GHz water line: broadening and shifting by air, N_2 and O_2 and integral intensity measurements" *Journal of Molecular Spectroscopy*, **218,** 2003, pp. 239-245.

[87] L. Rothman et al., "The HITRAN 2004 Molecular Spectroscopic Database," Journal of Quantitative Spectroscopy and Radiative Transfer, 96, 2005, pp. 139-204.

[88] T. P. Ackerman, and G. M. Stokes, "The Atmospheric Radiation Measurement Program," *Physics Today*, **56**, 1, 2003, pp. 38-44.

[89] J. Güldner and D. Spänkuch, "Remote Sensing of the Thermodynamic State of the Atmospheric Boundary Layer by Ground-Based Microwave Radiometry," *Journal of Atmospheric and Oceanic Technology*, **18**, 2001, pp. 925-933.

[90] A. Lüdi, L. Martin and C. Mätzler, "The Retrieval of Temperature Profiles with the Ground-Based Radiometer System ASMUWARA," IAP Research Report No. 2003-13, Sept. 2003.

[91] L. Martin, "ASMUWARA - The All-Sky Multi Wavelength Radiometer: Documentation," IAP Research Report, No. 2002-12, University of Bern, August 2002.

[92] G. M. Stokes, and S. E. Schwartz, "The Atmospheric Radiation Measurement (ARM) Program: Programmatic Background and Design of the Cloud and Radiation Testbed," *Bulletin of the American Meteorological Society,* **75**, 1994:, pp.1201-1221.

[93] A. S. Frisch, G. Feingold, C. W. Fairall, T. Uttal, and J. B. Snider, "On Cloud Radar and Microwave Measurements of Stratus Cloud Liquid Water Profiles," *Journal of Geophysical Research*, **103**, 1998, pp. 23195-23197.

[94] U. Löhnert, S. Crewell, and C. Simmer,: "An Integrated Approach towards Retrieving Physically Consistent Profiles Of Temperature, Humidity and

Cloud Liquid Water," *Journal of Applied Meteorology,* **43**, 9, 2004, pp. 1295-1307.

[95] B. B. Stankov, B. E. Martner, and M.K. Politovich, "Moisture Profiling of the Cloudy Winter Atmosphere using Combined Remote Sensors," *Journal of Atmospheric and Oceanic Technolog*y, **12**, 1995, pp. 488-510.

[96] B. B. Stankov, E.R. Westwater, and E.E. Gossard, "Use of Wind Profiler Estimates of Significant Moisture Gradients to Improve Humidity Profile Retrieval," *Journal of Atmospheric and Oceanic Technology*, **13**, 6, 1996, pp.1285-1290.

[97] Y. Han and E. R. Westwater, "Remote sensing of tropospheric water vapor and cloud liquid water by integrated ground-based sensors," *Journal of Atmospheric Oceanic Technology*, **12,5,** 1995, pp.1050-1059.

[98] F. S. Marzano, D. Cimini, P. Ciotti, and R. Ware, "Modeling and Measurement of Rainfall by Ground-based Multispectral Microwave Radiometry,*" IEEE Transactions on Geoscience and Remote Sensing,* **43**, 5, 2005, pp. 1000-1011.

[99] T. Nehrkorn and C. Grassotti, "Mesoscale Variational Assimilation of Profiling Radiometer Data," *16th Conference on Numerical Weather Prediction*, Seattle, WA, American Meteorological Society, 2004.

[100] J. Cermak, M. Schneebeli, D. Nowak, L. Vuilleumier, and J. Bendix, "Characterization of low clouds with satellite and ground-based remote sensing systems", TUC special issue, *Meteorologische Zeitschrift*, in press (2006).

[101] D. Cimini, T. J. Hewison, L. Martin, "Comparison of brightness temperatures observed from ground-based microwave radiometers during TUC", TUC special issue, *Meteorologische Zeitschrift*, in press (2006).

[102] D. Cimini, T. Hewison, L. Martin, J. Güldner, C. Gaffard, and F.S. Marzano, "Temperature and humidity profile retrievals from ground-based microwave radiometers during TUC", TUC special issue, *Meteorologische Zeitschrift*, in press (2006).

[103] T. Hewison, D. Cimini, L. Martin, C. Gaffard, and J. Nash: "Validating clear air absorption models using ground-based microwave radiometers and vice-versa", TUC special issue, *Meteorologische Zeitschrift*, in press (2006).

[104] L. Martin, M. Schneebeli, and C. Mätzler, "ASMUWARA, a ground-based radiometer system for tropospheric monitoring", TUC special issue, *Meteorologische Zeitschrift*, in press (2006).

[105] L. Martin., M. Schneebeli, and C. Mätzler, "Tropospheric water and temperature retrieval for ASMUWARA", TUC special issue, *Meteorologische Zeitschrift*, in press (2006).

[106] L. Martin, C. Mätzler, T. Hewison, and D. Ruffieux: "Intercomparison of integrated water vapour measurements", TUC special issue, *Meteorologische Zeitschrift*, in press (2006).